Geophysical Journal International

Geophys. J. Int. (2012) **189,** 937–955 doi: 10.1111/j.1365-246X.2012.05434.x

Coseismic deflection change of the vertical caused by the 2011 Tohoku-Oki earthquake (M_w 9.0)

Wenke Sun and Xin Zhou

Key Laboratory of Computational Geodynamics, Graduate University of Chinese Academy of Sciences, China. E-mail: sunw@gucas.ac.cn

Accepted 2012 February 23. Received 2012 February 23; in original form 2011 January 18

SUMMARY

This paper presents a scheme to compute coseismic deflection change, and presents a set of Green's functions for four independent dislocation sources. To compare the theoretical deflection changes with the GRACE-observed ones, the dislocation Love numbers are truncated and the Green's functions are computed with application of a Gaussian filter. Using this computing scheme, the modelled coseismic geoid and deflection changes can be compared directly with the GRACE-observed ones. Numerical computation and comparison show that the computing scheme is valid and efficient, and that it can obviate much unnecessary computing time for high-degree Love numbers. This study further examines the problem of sea water correction to modelled geoid and deflection changes because it is an important and necessary step to compare the modelled results with GRACE-observed deformations. As an application of the dislocation theory and the computing scheme described as a result of this study, we consider the 2011 Tohoku-Oki earthquake (M_w 9.0) using three different fault-slip models. Using the fault models, we compute the coseismic geoid and deflection changes for an area around Japan, considering sea water corrections. Results indicate that the coseismic geoid and deflection changes can be detected clearly by GRACE observation, and the coseismic geoid change is not sensitive to the fault-slip models: the three slip models yield identical coseismic geoid changes; whereas the coseismic deflection changes are very sensitive to the fault-slip models because the modelled deflection changes indicate pretty large difference, especially for the E–W component. These behaviours provide us a new and useful approach to invert seismic faults using GRACE-observed deflection changes as constraints.

Key words: Satellite geodesy; Satellite gravity; Space geodetic surveys; Gravity anomalies and Earth structure; Geopotential theory.

1 INTRODUCTION

To interpret observed coseismic deformations such as displacement, strain, tilt and gravity change, scientists have presented different dislocation theories for different earth models, such as theories for half-space media by Okada (1985), Okubo (1991, 1992) and Wang *et al.* (2006) among others. These theories are mathematically simple and are widely used in practical applications in modelling coseismic deformation even today.

For a more realistic Earth model such as the Preliminary Reference Earth Model (PREM) (Dziewonski & Anderson 1981), Rundle (1982) studied viscoelastic gravitational deformation by a rectangular thrust fault in a layered Earth. Pollitz (1992) solved the problem of regional displacement and strain fields induced by dislocation in a viscoelastic, non-self-gravitating model. Sun's team (Sun 1992a,b; Sun & Okubo 1993; Sun *et al.* 1996; Sun *et al.*2006; Sun *et al.* 2009) studied the surface displacement, strain, potential and gravity changes caused by dislocations in spherically symmetrical Earth models. Their results showed that the Earth's sphericity can cause a 10 per cent difference when the epicentral distance is greater than 10°; radial heterogeneity should be considered when the epicentral distance is greater than 0.5°. Okubo (1993) proposed a reciprocity theorem for connecting solutions of the dislocation and tidal, shear and load deformations, finding that the deformation on surface $r = a$ caused by dislocations at $r = r_s$ is expressible simply by a linear combination of the tide, load and shear solutions at $r = r_s$. Ma & Kusznir (1994) modified elastic dislocation theory to derive subsurface displacements for faults in a three-layer elastic-gravitational medium and its application to examine coseismic and post-seismic surface and subsurface displacement during continental extensional faulting. Piersanti *et al.* (1995), Sabadini *et al.* (1995) and Soldati *et al.* (1998) studied the gravity, displacement and rates induced by a dislocation in viscoelastic, stratified Earth models, accounting for sphericity and self-gravitation using a self-consistent approach. They produced results of surface displacement and velocities in the near field and far field for various viscosity profiles in the mantle. Tanaka *et al.* (2006) studied that problem using a new method that overcomes some previous numerical difficulties and which guarantees accuracy.

Remarkable coseismic displacements have been observed frequently in the last several decades before and after great earthquakes such as the Taiwan Chi–Chi earthquake (M_w 7.6) in 1999 (Yang *et al.* 2000; Yu *et al.* 2001), the Kunlun earthquake (M_w 7.8) in 2001 (Lin *et al.* 2002) and the Tokachi-Oki earthquake (M_w 8.0) in 2003 (Imanishi *et al.* 2004; Irwan *et al.* 2004). These observations indicate that the dominating deformations appear in the near field and attenuate rapidly with increased epicentral distance. In addition, coseismic deformations in the far field caused by huge earthquakes have been observed using modern geodetic techniques. For example, the coseismic horizontal displacement changes caused by the Sumatra–Andaman earthquake (M_w 9.3) were detected using GPS data in Japan about 4500 km distant from the epicentre (Ammon *et al.* 2005; Banerjee *et al.* 2005; Khan & Gudmundsson 2005; Vigny *et al.* 2005; Boschi *et al.* 2006; Fu & Sun 2006). All these observations imply that coseismic deformation accompanying the Sumatra–Andaman earthquake occurs not only near the epicentre, but over the entire earth. For that reason, we are compelled to investigate global coseismic deformations using both a theoretical model and practical observation. Especially, to interpret the observed geodetic and geophysical changes, a spherical dislocation theory is regarded as necessary to model/inverse the fracture fault and to calculate the coseismic deformations over the earth surface.

The coseismic gravity field changes are similarly detectable by gravity measurement. For example, coseismic gravity changes generated by the Tokachi-Oki earthquake in 2003 were detected using superconducting gravimeters (Imanishi *et al.* 2004). Furthermore, according to Gross & Chao (2001), Sun & Okubo (2004) and Mikhailov *et al.* (2004), the satellite gravity mission GRACE is theoretically able to detect the coseismic gravity changes caused by a giant earthquake with magnitude of 8 or greater. Subsequently, the coseismic and post-seismic gravity changes caused by 2004 Sumatra–Andaman earthquake (M_w 9.3) were detected by GRACE (Han *et al.* 2006; Chen *et al.* 2007; Ogawa & Heki 2007; Panet *et al.* 2007; Cannelli *et al.*2008; De Linage *et al.* 2009). Recently, coseismic gravity changes reportedly caused by the 2010 Chile earthquake (M_w 8.8) were detected again by GRACE (Han *et al.* 2010; Heki & Matsuo 2010; Zhou *et al.* 2011b). Matsuo & Heki (2011) reported that the GRACE detected gravity change caused by the 2011 Tohoku-Oki earthquake (M_w 9.0). Therefore, to interpret the observed deformation and to reflect the effects of the earth curvature and vertical structure, the dislocation for spherical earth model is important and necessary (Sun *et al.* 2009; Zhou *et al.* 2011a).

The Tohoku-Oki earthquake (M_w 9.0), which occurred near the east coast of Honshu on 2011 March 11, provided an opportunity for scientists to study coseismic deformations using modern geodetic data. This event was the fourth largest recorded in the world over the last century. It generated huge tsunami and caused an unprecedented catastrophe to Japan, and the destruction of nuclear power facilities. The GPS data show that the giant earthquake permanently changed Honshu's surface and coastline. The east coast moved eastward with a maximum value of more than 4 m, and sank about 1 m (Geospatial Information Authority of Japan, 2011). After the quake, some researchers presented different fault-slip models inversed from seismic waveform data, GPS observation deformations or both data combination, such as models by Hayes (2011), Shao *et al.* (2011) and Wei *et al.* (2011). Zhou *et al.* (2011a) compared the three slip models using dislocation theories for half-space and spherical earth models, and GPS data in both the near (Japan) and far field (China). They found that the modelled coseismic displacement calculated using spherical dislocation theory (Sun *et al.* 2009) with the Shao *et al.* (2011) slip model fits the GPS-observed results better than either of the other two models.

In 2002, GRACE was launched by GFZ (GeoForschungsZentrum) and NASA (National Aeronautics and Space Administration) to provide global gravity model and to study the global water cycle. It can also be used to study earthquake from space. It was successfully used to detect coseismic gravity changes resulting from the 2004 Sumatra earthquake (M_w 9.3) and the 2010 Chile earthquake (M_w 8.8; Han *et al.* 2006; Chen *et al.* 2007; Ogawa & Heki 2007; Panet *et al.* 2007; De Linage *et al.* 2009; Han *et al.* 2010; Heki & Matsuo 2010; Zhou *et al.* 2011b). The Tohoku earthquake (M_w 9.0) is intermediate of the 2004 Sumatra and 2010 Chile earthquakes in magnitude. Therefore, it is expected to have been detected by GRACE also. Zhou *et al.* (2011b) found that the coseismic gravity change was detectable by GRACE.

Actually, GRACE provides us a global potential model for each month. It is not only to be used to compute gravity and geoid changes, but also to compute the vertical deflection change. The vertical deflection is defined as the horizontal derivative of the geoid; it is expected to be more sensitive to coseismic deformation than a geoid. It can open a new approach to the study of coseismic deformation with GRACE data, because the differentiation of the GRACE geoids in the North–South direction that corresponds to the N–S vertical deflection change takes advantage of the higher precision along-track rather than across-track. This nicely appears when we compare the performance of earthquake signal recovery in terms of geoid or vertical deflection, and allows discriminating between different rupture models, showing the interest of GRACE for earthquake studies.

For this purpose, this study presents a new scheme to compute the deflection change of the vertical, with extending the current dislocation theory for a spherical earth model (Sun & Okubo 1993; Sun *et al.* 2009). We first derive a set of Green's functions for the coseismic deflection changes, which is useful to compute coseismic deflections caused by arbitrary earthquake occurred at any place. Then, as an application, the Green's functions are used to calculate coseismic geoid and deflection changes caused by the 2011 Tohoku-Oki earthquake (M_w 9.0) with the above three fault-slip models. Results show that this earthquake generated considerable coseismic geoid and deflection changes, and they were clearly detected by GRACE.

2 COSEISMIC GEOID AND DEFLECTION CHANGES FOR A POINT DISLOCATION

We define the dislocation model (as presented in fig. 1 of Sun *et al.* 2009) at radial distance r_s on an infinitesimal fault dS by slip vector ν, normal $\mathbf{n}$, slip angle λ and dip angle δ in the coordinate system ($\mathbf{e}_1, \mathbf{e}_2, \mathbf{e}_3$); unit vectors $\mathbf{e}_1$ and $\mathbf{e}_2$ are taken, respectively, in the equatorial plane in the directions of longitude $\varphi = 0$ and $\pi/2$, and $\mathbf{e}_3$ along polar axis $\mathbf{r}$. Relative movement (dislocation) of the two fault sides is defined as $(U/2) - (-U/2) = U$. Based on the definitions presented above, Sun *et al.* (2009) presented the generalized expression of the Green's functions of displacement, strain, potential and gravity changes. In the following, we present Green's functions of coseismic deflection change of the vertical by following its scheme. Readers can refer to it for details that are omitted here.

If dislocation occurs in a spherical earth, such as in a homogeneous sphere or an Spherical, Non-Rotating, perfectly Elastic and

Isotropic (SNREI) earth (Dahlen 1968), then the excited geopotential change $\psi(r, \theta, \varphi)$ is describable as

$$\psi(r, \theta, \varphi) = \sum_{n,m,i,j} k^{n,ij}_{5,m}(r) Y^m_n(\theta, \varphi) \cdot \nu_i n_j \frac{g_0 U dS}{a^2}, \tag{1}$$

where $Y^m_n(\theta, \varphi) = P^m_n(\cos\theta) e^{im\varphi}$, $P^m_n(\cos\theta)$ denotes the associated Legendre's function, a stands for the earth radius and g_0 represents the acceleration of gravity on the Earth surface. In addition, $k^{n,ij}_{5,m}(a)$ signifies the dislocation Love number (dimensionless) of coseismic potential change, defined as $k^{n,ij}_{5,m}(a) = y^{n,ij}_{5,m}(a) \cdot a^2/g_0$ (Sun 1992a,b; Sun & Okubo 1993). The y-variables $y^{n,ij}_{5,m}(a)$ are obtainable by solving the linearized first-order equations of equilibrium, stress–strain relation and Poisson's equation for excited deformation (Saito 1967; Takeuchi & Saito 1972). The toroidal deformation has no contribution to potential change and deflection change of the vertical.

$$\dot{\mathbf{Y}} = \mathbf{A}\mathbf{Y}. \tag{2}$$

In that equation, $\mathbf{Y} = (y^{n,ij}_{1,m}, \cdots, y^{n,ij}_{6,m})^T$, and dot '.' represents the derivative with respect to r ; $y^{n,ij}_{1,m}$ and $y^{n,ij}_{3,m}$ respectively express the radial function of the vertical and horizontal displacement. $y^{n,ij}_{2,m}$ and $y^{n,ij}_{4,m}$ respectively denote the vertical and horizontal stress components. $y^{n,ij}_{5,m}$ is the potential change and $y^{n,ij}_{6,m}$ is the variable related with $y^{n,ij}_{1,m}$ and $y^{n,ij}_{5,m}$ defined by Takeuchi & Saito (1972). In addition, $\mathbf{A}$ is the coefficient matrix depending on the earth model. Solutions $\mathbf{Y}$ satisfy the discontinuity condition across the radius of the source $r = r_s$ (Saito 1967, 1974), as

$$\mathbf{S} = [\mathbf{Y}(r_s + 0) - \mathbf{Y}(r_s - 0)]\, \delta(r - r_s). \tag{3}$$

Vector $\mathbf{S} = (s^{n,ij}_{1,m}, \cdots, s^{n,ij}_{6,m})^{\mathrm{T}}$ represents spheroidal source functions. Only spherical orders $|m| \leq 2$ are involved because the source is taken on the polar axis.

To solve eq. (2) with the discontinuity condition eq. (3) and the following free boundary conditions

$$\forall n, m, i, j : y^{n,ij}_{2,m}(a) = y^{n,ij}_{4,m}(a) = y^{n,ij}_{6,m}(a) = 0, \tag{4}$$

several methods have been proposed and discussed by Smylie & Mansinha (1971), Takeuchi & Saito (1972) and Sun & Okubo (1993). Details of their applications are discussed in Sun (1992a,b) and Sun & Okubo (1993).

Because $i = 1, 2, 3$ and $j = 1, 2, 3$, the combination of i and j is 9. Consequently, the total solutions of all y should be nine. However, because of the symmetry of source functions $\mathbf{S}$, we have $y^{n,ij}_{k,m} = y^{n,ji}_{k,m}$ because $\mathbf{S}$ are invariant by interchanging i and j. Therefore, the number of solutions of $y^{n,ij}_{k,m}(a)$ reduces to six. Furthermore, intrinsic symmetry within the fault geometry indicates that components $y^{n,11}_{k,m}(a)$and $y^{n,31}_{k,m}(a)$ are calculable by application of rotational transformation about the polar axis to $y^{n,22}_{k,m}(a)$ and $y^{n,32}_{k,m}(a)$. Finally, the number of independent solutions of $y^{n,ij}_{k,m}(a)$ is four, meaning that if any four independent solutions are obtained, then the other solutions among the nine are also readily obtainable. For this study, we choose ($y^{n,12}_{k,m}$,$y^{n,32}_{k,m}$,$y^{n,22}_{k,m}$,$y^{n,33}_{k,m}$) as four independent solutions. They are excited, respectively, by a vertical strike-slip, a vertical dip-slip, a horizontal opening along a vertical fault and a vertical opening along a horizontal fault. Once solutions $y^{n,ij}_{k,m}(a)$ of eq. (2) are obtained numerically, any coseismic deformation can be derived and calculated numerically.

After solutions of $y^{n,ij}_{5,m}$ are obtained for source functions (Saito 1967), the dislocation Love number $k^{n,ij}_{5,m}(a)$ can be determined, so that the corresponding coseismic geoid and deflection vertical changes can be derived as presented below (Sun & Okubo 1993; Sun *et al.* 2009).

$$N(a, \theta, \varphi) = \frac{\psi(a, \theta, \varphi)}{g_0}, \tag{5}$$

$$\xi(a, \theta, \varphi) = \frac{1}{a} \frac{\partial N(a, \theta, \varphi)}{\partial \theta}, \tag{6}$$

$$\eta(a, \theta, \varphi) = -\frac{1}{a \sin\theta} \frac{\partial N(a, \theta, \varphi)}{\partial \varphi}. \tag{7}$$

Considering the definition of potential change $\psi(a, \theta, \varphi)$ in eq. (1), the above geoid and deflection changes can be written further as follows.

$$N(a, \theta, \varphi) = \sum_{n,m,i,j} k^{n,ij}_{5,m}(a) \frac{\nu_i n_j U dS}{a^2}, \tag{8}$$

$$\xi(a, \theta, \varphi) = \sum_{n,m,i,j} k^{n,ij}_{5,m}(a) \frac{\partial Y^m_n(\theta, \varphi)}{\partial \theta} \cdot \frac{\nu_i n_j U dS}{a^3}, \tag{9}$$

$$\eta(a, \theta, \varphi) = -\sum_{n,m,i,j} k^{n,ij}_{5,m}(a) \frac{\partial Y^m_n(\theta, \varphi)}{\sin\theta \partial \varphi} \cdot \frac{\nu_i n_j U dS}{a^3}. \tag{10}$$

Because the expressions of coseismic geoid change were already described in Sun *et al.* (2009), we will mainly discuss the north–south and east–west components of the deflection of the vertical changes below. Using the same scheme of Sun *et al.* (2009), the eqs (9) and (10) can be rearranged as

$$\xi(a, \theta, \varphi) = \sum_{i,j} \xi^{ij}(a, \theta, \varphi) \cdot \frac{\nu_i n_j U dS}{a^3} \tag{11}$$

and

$$\eta(a, \theta, \varphi) = \sum_{i,j} \eta^{ij}(a, \theta, \varphi) \cdot \frac{\nu_i n_j U dS}{a^3}, \tag{12}$$

where

$$\xi^{ij}(a, \theta, \varphi) = \sum_{n,m} k^{n,ij}_{5,m}(a) \frac{\partial Y^m_n(\theta, \varphi)}{\partial \theta} \tag{13}$$

and

$$\eta^{ij}(a, \theta, \varphi) = -\sum_{n,m} \frac{k^{n,ij}_{5,m}(a)}{\sin\theta} \frac{\partial Y^m_n(\theta, \varphi)}{\partial \varphi} \tag{14}$$

respectively stand for the north–south and east–west components of the deflection vertical changes for the nine (four independent) individual source functions.

If we define Green's functions of the coseismic deflection changes for the four independent components as the following:

$$\hat{\xi}^{12}(a, \theta) = -2 \sum_{n=2}^{\infty} k^{n,12}_{5,2}(a) \frac{\partial P^2_n(\cos\theta)}{\partial \theta}, \tag{15}$$

$$\hat{\xi}^{32}(a, \theta) = -2 \sum_{n=2}^{\infty} k^{n,32}_{5,1}(a) \frac{\partial P^1_n(\cos\theta)}{\partial \theta}, \tag{16}$$

$$\hat{\xi}^{22,0}(a, \theta) = \sum_{n=2}^{\infty} k^{n,22}_{5,0}(a) \frac{\partial P_n(\cos\theta)}{\partial \theta}, \tag{17}$$

$$\hat{\xi}^{33}(a,\theta)=\sum_{n=2}^{\infty}k_{5,0}^{n,33}(a)\frac{\partial P_n(\cos\theta)}{\partial\theta}, \tag{18}$$

$$\hat{\eta}^{12}(a,\theta)=2\sum_{n=2}^{\infty}2k_{5,2}^{n,12}(a)\frac{P_n^2(\cos\theta)}{\sin\theta}, \tag{19}$$

$$\hat{\eta}^{32}(a,\theta)=2\sum_{n=2}^{\infty}k_{5,1}^{n,32}(a)\frac{P_n^1(\cos\theta)}{\sin\theta}, \tag{20}$$

$$\hat{\eta}^{22,0}(a,\theta)=0, \tag{21}$$

$$\eta^{33}(a,\theta)=0, \tag{22}$$

then the four independent solutions of the north–south and east–west components of the deflection vertical changes become the following:

$$\xi^{12}(a,\theta,\varphi)=\hat{\xi}^{12}(a,\theta)\sin 2\varphi, \tag{23}$$

$$\xi^{32}(a,\theta,\varphi)=\hat{\xi}^{32}(a,\theta)\sin\varphi, \tag{24}$$

$$\xi^{22,0}(a,\theta,\varphi)=\hat{\xi}^{22,0}(a,\theta), \tag{25}$$

$$\xi^{33}(a,\theta,\varphi)=\hat{\xi}^{33}(a,\theta), \tag{26}$$

$$\eta^{12}(a,\theta,\varphi)=\hat{\eta}^{12}(a,\theta)\cos 2\varphi, \tag{27}$$

$$\eta^{32}(a,\theta,\varphi)=\hat{\eta}^{32}(a,\theta)\cos\varphi, \tag{28}$$

$$\eta^{22,0}(a,\theta,\varphi)=0, \tag{29}$$

$$\eta^{33}(a,\theta,\varphi)=0. \tag{30}$$

These Green's functions in eqs (15)–(22) are useful to calculate the coseismic deflection of the vertical changes excited by four types of independent sources buried in a spherically symmetric earth model. In combination, these components allow calculation of a displacement field that is excited by an arbitrary seismic source.

To apply the above four independent solutions to a practical event, we consider an inclined dislocation on the polar axis with the fault line in the direction of Greenwich meridian. A dislocation vector ν and its normal $\mathbf{n}$ are expressible in terms of slip angle λ, and dip angle δ of the fault as presented below.

$$\begin{aligned}\mathbf{n}&=-\mathbf{e}_2\sin\delta+\mathbf{e}_3\cos\delta,\\ \nu&=\mathbf{e}_1\cos\lambda+\mathbf{e}_2\cos\delta\sin\lambda+\mathbf{e}_3\sin\delta\sin\lambda.\end{aligned} \tag{31}$$

We have a shear dislocation problem if the dislocation vector ν runs parallel to the fault plane. In this case, the excited coseismic displacement vector is expressible using the above displacement components of the four independent sources as the following (herein Θstands for either ξ or η).

$$\begin{aligned}\Theta^{s}(a,\theta,\varphi)&=\Theta^{ij}(a,\theta,\varphi)\nu_i n_j\frac{UdS}{a^2}\\ &=\left\{\cos\lambda\left[\Theta^{12}\sin\delta-\Theta^{13}\cos\delta\right]\right.\\ &\quad\left.+\sin\lambda\left[\frac{1}{2}\left(\Theta^{33}-\Theta^{22}\right)\sin 2\delta-\Theta^{32}\cos 2\delta\right]\right\}\frac{UdS}{a^2},\end{aligned} \tag{32}$$

where the component $\Theta^{13}(a,\theta,\varphi)$ can be expressed by $\Theta^{32}(a,\theta,\varphi)$as

$$\Theta^{13}(a,\theta,\varphi)=\Theta^{32}\left(a,\theta,\varphi+\frac{\pi}{2}\right). \tag{33}$$

For a tensile opening, the slip vector and the normal become equal.

$$\nu=\mathbf{n}=-\mathbf{e}_2\sin\delta+\mathbf{e}_3\cos\delta. \tag{34}$$

In this case, the excited coseismic strain is obtainable as the following:

$$\begin{aligned}\Theta^{t}(a,\theta,\varphi)&=\Theta^{ij}(a,\theta,\varphi)\nu_i n_j\frac{UdS}{a^2}\\ &=\left(\Theta^{33}\cos^2\delta+\Theta^{22}\sin^2\delta+\Theta^{32}\sin 2\delta\right)\frac{UdS}{a^2}.\end{aligned} \tag{35}$$

The dislocation is not necessarily on the polar axis nor is the fault line along the Greenwich meridian. In practice, we might derive formulae for an inclined dislocation at an arbitrary point by application of a geometrical rotation to the results described above. Practical treatment is exactly the same as that for coseismic displacement, strain and gravity changes (for details refer Sun & Okubo 1993 and Sun *et al.* 2009).

3 NUMERICAL COMPUTATION OF THE GREEN'S FUNCTIONS WITH A GAUSSIAN FILTER

The theoretical expressions presented herein are useful to interpret the GRACE-observed data. Because of the limited spatial resolution of GRACE measurement, usually a filter such as the Gaussian filter is used to smooth the GRACE data. To compare the observed coseismic deformation, for example, coseismic gravity change, geoid change and deflection change of the vertical, the modelled coseismic deformations must be filtered similarly. Therefore, when the theoretical formulae above are used to compute coseismic geoid and vertical deflection changes, the corresponding results must also be filtered. Usually, one first computes the coseismic deformations according to a dislocation theory and a seismic slip model; then one applies a filter to the modelled results (e.g. Sun *et al.* 2009; Zhou *et al.* 2011a). In this computing scheme, all y-solutions of $y_{k,m}^{n,ij}(a)$ (dislocation Love Number) must be involved in the numerical computation, where the harmonic degree n must be sufficiently large to guarantee convergence of the Green's functions; although for a very shallow source, the truncation of dislocation Love numbers $k_{5,m}^{n,ij}(a)$ goes to a large number N. For example, when source depth $d=1$ km, the truncation should be made at $N=63700$; when source depth $d=20$ km, the truncation number is $N=3185$. Fig. 1 shows the normalized dislocation Love numbers $k_{5,m}^{n,ij}(a)$ with truncation at $N=3185$. The corresponding Green's functions should be calculated by summing up these dislocation Love numbers. Consequently, many numerical computations should be made, costing much computation time. The problem is that the high-frequency part of the dislocation numbers has no contribution after the filter is applied.

To reduce the unnecessary computation time on dislocation Love numbers and Green's functions, we might consider applying the Gaussian filter to the dislocation Love numbers, so that the Green's functions of coseismic deflection change of the vertical becomes the following:

$$\xi_w^{ij}(a,\theta,\varphi)=\sum_{n,m}k_{5,m}^{n,ij}(a)w_n\frac{\partial Y_n^m(\theta,\varphi)}{\partial\theta}, \tag{36}$$

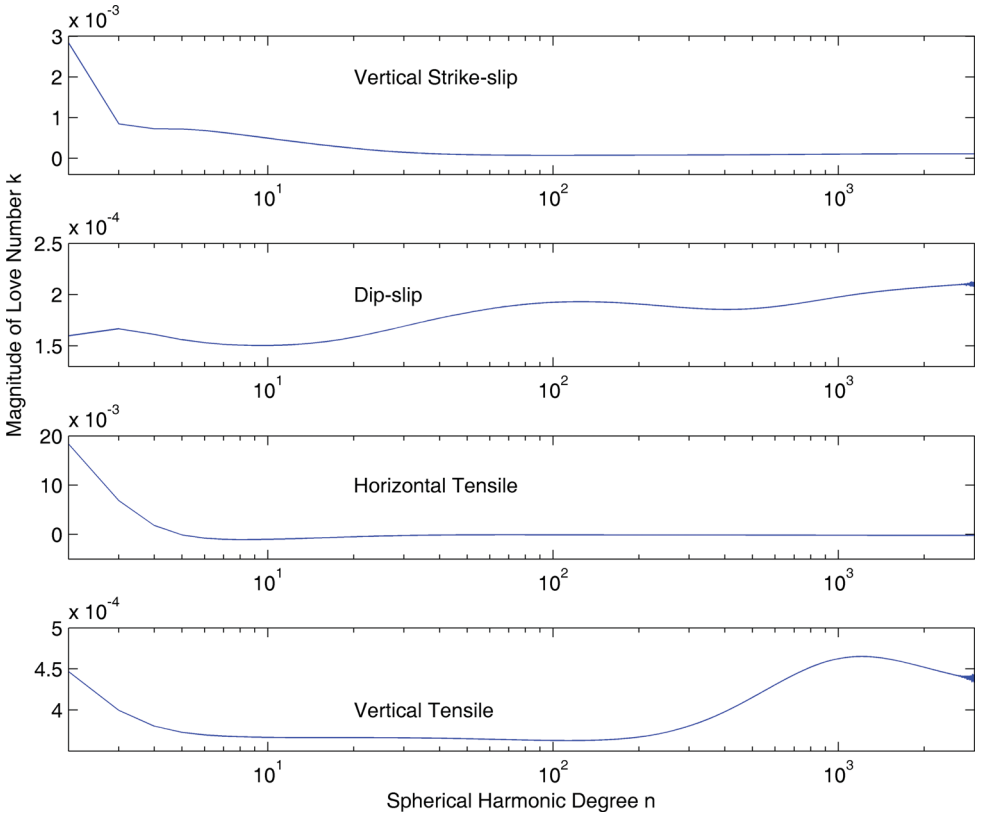

Figure 1. Dislocation Love numbers $k_{5,m}^{n,ij}(a)$ for the four types of independent seismic sources: vertical strike-slip, dip-slip, horizontal tensile and vertical tensile. To guarantee the accuracy of the Green's functions, the dislocation Love numbers must be truncated at $N = 3185$.

$$\eta_w^{ij}(a,\theta,\varphi) = -\sum_{n,m} \frac{k_{5,m}^{n,ij}(a)}{\sin\theta} w_n \frac{\partial Y_n^m(\theta,\varphi)}{\partial\varphi}. \tag{37}$$

Therein, w_n is a spectral form of the Gaussian filter (Jekeli 1981; Wahr *et al.* 1998). It can be computed with recursion relations as shown below:

$$w_0 = 1, \tag{38}$$

$$w_1 = \frac{1+e^{-2b}}{1-e^{-2b}} - \frac{1}{b}, \tag{39}$$

$$w_{n+1} = -\frac{2n+1}{b} w_n + w_{n-1}, \tag{40}$$

$$b = \frac{\ln(2)}{1-\cos(r/a)}. \tag{41}$$

In those equations, r represents the averaging radius and a stands for the radius of the earth. The spherical harmonic coefficients w_n of Gaussian filter (Fig. 2) show that the coefficients decrease quickly as harmonic degree n increases. When $n = 140$, w_n already drops to 7 orders smaller.

After applying the Gaussian filter w_n to the dislocation Love numbers, we obtain new filtered dislocation Love numbers as shown below:

$$\bar{k}_{5,2}^{n,12}(a) = k_{5,2}^{n,12}(a) w_n, \tag{42}$$

$$\bar{k}_{5,1}^{n,32}(a) = k_{5,1}^{n,32}(a) w_n, \tag{43}$$

$$\bar{k}_{5,0}^{n,22}(a) = k_{5,0}^{n,22}(a) w_n, \tag{44}$$

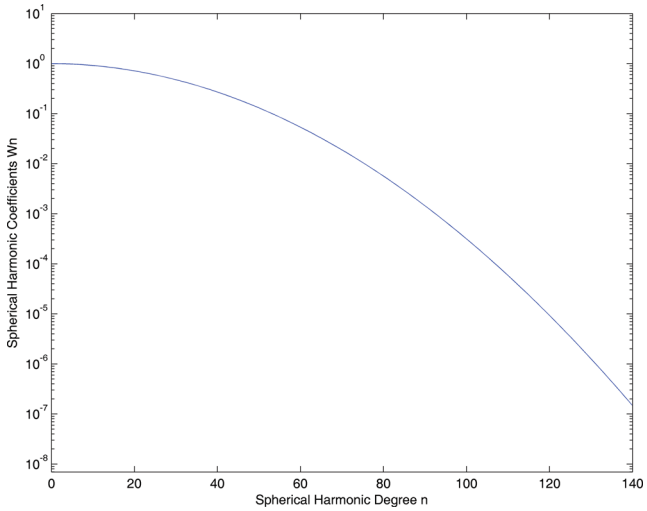

Figure 2. Spherical harmonic coefficients w_n of Gaussian filter with averaging radius of 300 km. The coefficients decrease quickly as the degree of harmonic n increases.

$$\bar{k}_{5,0}^{n,33}(a) = k_{5,0}^{n,33}(a) w_n. \tag{45}$$

Because of the rapid convergence behaviour as shown above, the filter dislocation Love numbers $\bar{k}_{5,m}^{n,ij}(a)$ drops to almost zero at $n = 140$, as depicted in Fig. 3. This property implies that we might only compute dislocation Love numbers for $n \leq 140$, no matter how deep the source depth is. Even for the 1 km seismic source, we might only consider the dislocation Love numbers for $n \leq 140$ instead of $n = 63700$.

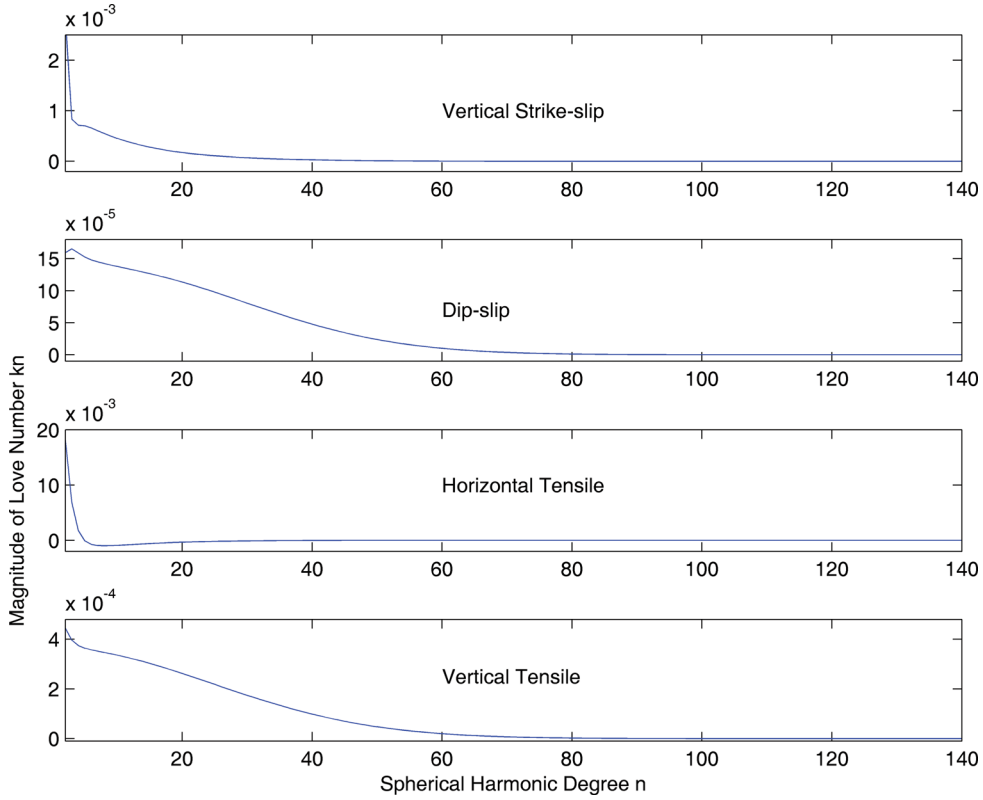

Figure 3. Smoothed dislocation Love numbers $\bar{k}^{n,ij}_{5,m}(a)$ by the Gaussian filter.

With consideration of the current maximum degree ($n = 120$) of the GRACE derived potential model, we might practically compute each component of the Green's functions as shown below:

$$\hat{\xi}^{12}_w(a,\theta) = -2\sum_{n=2}^{120} \bar{k}^{n,12}_{5,2}(a)\frac{\partial P^2_n(\cos\theta)}{\partial\theta}, \tag{46}$$

$$\hat{\xi}^{32}_w(a,\theta) = -2\sum_{n=2}^{120} \bar{k}^{n,32}_{5,1}(a)\frac{\partial P^1_n(\cos\theta)}{\partial\theta}, \tag{47}$$

$$\hat{\xi}^{22,0}_w(a,\theta) = \sum_{n=2}^{120} \bar{k}^{n,22}_{5,0}(a)\frac{\partial P_n(\cos\theta)}{\partial\theta}, \tag{48}$$

$$\hat{\xi}^{33}_w(a,\theta) = \sum_{n=2}^{120} \bar{k}^{n,33}_{5,0}(a)\frac{\partial P_n(\cos\theta)}{\partial\theta}, \tag{49}$$

$$\hat{\eta}^{12}_w(a,\theta) = 2\sum_{n=2}^{120} 2\bar{k}^{n,12}_{5,2}(a)\frac{P^2_n(\cos\theta)}{\sin\theta}, \tag{50}$$

$$\hat{\eta}^{32}_w(a,\theta) = 2\sum_{n=2}^{120} \bar{k}^{n,32}_{5,1}(a)\frac{P^1_n(\cos\theta)}{\sin\theta}, \tag{51}$$

$$\hat{\eta}^{22,0}_w(a,\theta) = 0, \tag{52}$$

$$\eta^{33}_w(a,\theta) = 0. \tag{53}$$

To verify the validity of the computing scheme above, we compare in Fig. 4 the coseismic geoid changes caused by the 2011 Tohoku-Oki earthquake (M_w 9.0), calculated (1) using conversional Green's functions to integrate over the fault area, and filter the modelled geoid change with Gaussian filter ($r = 300$km; Fig. 4a) and (2) using the same filtered ($r = 300$km) Green's functions and then integration finally (Fig. 4b). The comparison shows that the geoid changes calculated using the two schemes are similar, which implies that the computing explained scheme above is valid and efficient. To observe how the two results agree, their difference is plotted in Fig. 4(c). It is seen that the maximum difference is about 0.1 mm, which is considered caused by the numerical error.

4 THREE FAULT PLAN MODELS OF THE 2011 TOHOKU-OKI EARTHQUAKE (M_w 9.0)

As a numerical application, in this study, we consider the 2011 Tohoku-Oki earthquake, with three fault-slip models for comparison. Fig. 5 gives the three slip models given by (1) Shao *et al.* (2011), (2) Wei *et al.* (2011) and (3) Hayes (2011). Shao *et al.* (2011) presented a finite fault model (called the UCSB model) consisting of 19 × 10 subfaults (25 km × 20 km cell size) with strike angle of 198° and dip angle of 10° (Fig. 5a) and with epicentre located at (38.05°N, 142.8°E) using the Global Seismographic Network (GSN) broad-band waveforms downloaded from the IRIS DMC and 28 teleseismic broadband *P* waveforms, 25 broadband *SH* waveforms and 54 long-period surface waves analysed. Wei *et al.* (2011) used the GSN broad-band data downloaded from the IRIS DMC and GPS data preliminary solution provided by the Advanced Range Instrumentation Aircraft (ARIA) team at the Jet Propulsion Laboratory (JPL) and Caltech to inverse the finite slip distribution

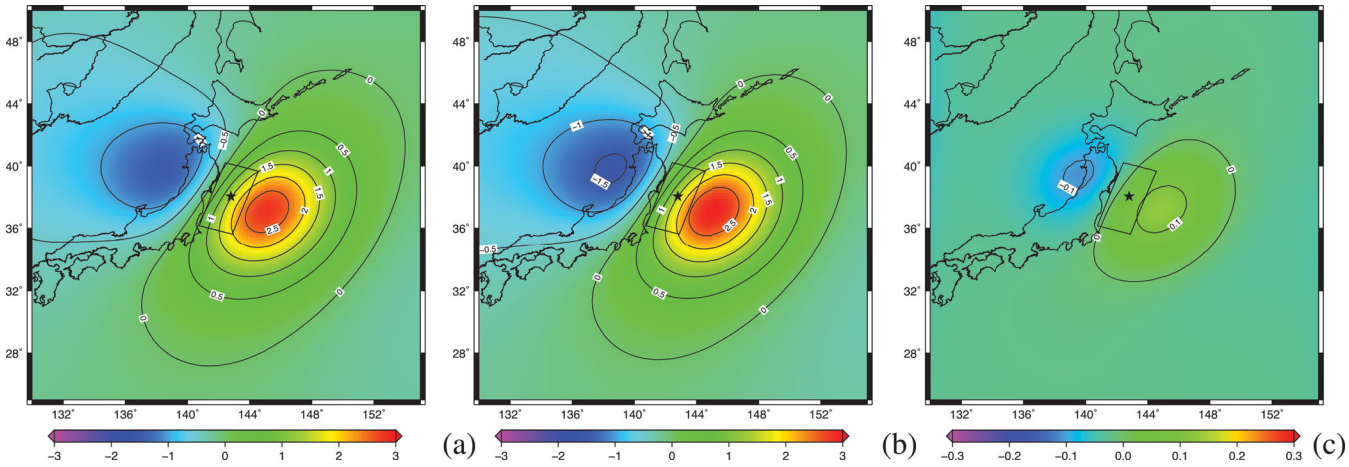

Figure 4. Comparison of the coseismic geoid changes caused by the 2011 Tohoku-Oki earthquake (M_w 9.0), calculated by (a) using conversional Green's functions to integrate over the fault area; then filter the modelled geoid change with Gaussian filter ($r = 300$km); (b) using the above filtered Green's functions and finally integration and (c) the difference between (a) and (b). The fault model of Shao *et al.* (2011) is used here. Unit: mm.

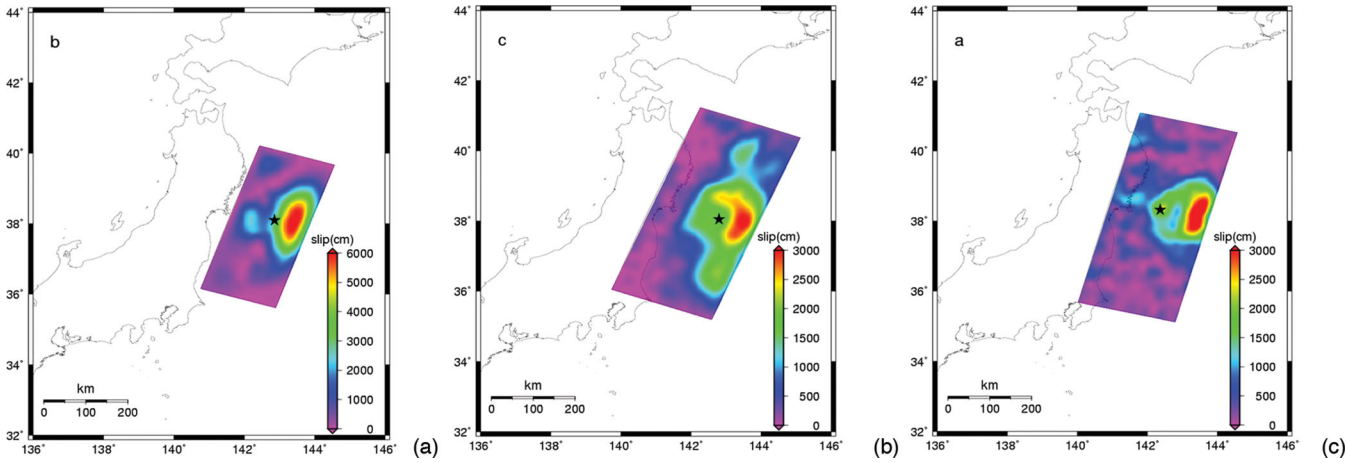

Figure 5. Three fault-slip models for the 2011 Tohoku earthquake reported by (a) Shao *et al.* (2011), (b) Wei *et al.* (2011) and (c) Hayes (2011). Black stars in (a)–(c) denote the three models' epicentres.

model (called the ARIA model). They analysed 27 teleseismic *P* waveforms and 21 *SH* waveforms and then inversed a finite fault model constrained by GPS observation. The model comprises 25 × 14 subfaults (25 km × 20 km cell size) with a strike angle of 201° and a dip angle of 9° (Fig. 5b). The Hayes' model (called the USGS model) is an updated version of the USGS model for the Tohoku earthquake (M_w 9.0), with the epicentre located at (38.32°N, 142.37°E). To obtain the finite slip model, Hayes *et al.* used the GSN broad-band waveforms downloaded from the National Earthquake Information Center (NEIC) to analyse 39 teleseismic broad-band *P* waveforms, 22 broadband *SH* waveforms and 55 long-period surface waves. The inversed finite fault comprises 25 × 13 subfaults, each of which has a 25 km × 20 km cell size, with a strike angle of 195° and a dip angle of 10° (Fig. 5c) and with epicentre located at (38.05°N, 142.8°E).

Fig. 5 shows that the seismic moment is almost identical for the three slip models, but the fault size and slip magnitude differ. Correspondingly, it is expected that the modelled displacements differ for the different slip models. Zhou *et al.* (2011a) compared the model displacements and the GPS-observed values, and found that the ARIA model agrees well with the observations, whether in the near field or far field.

5 SEA WATER CORRECTIONS TO MODELLED COSEISMIC DEFLECTION CHANGES OF THE VERTICAL

The dislocation theory above is valid for a solid elastic earth, and the corresponding computing program assumed dry earth, so that the surface subsidence on the earth surface is replaced with air. However, in practice, a large earthquake often occurs in an ocean or subduction area, as was true of the 2004 Sumatra earthquake (M_w 9.3) and the 2011 Tohoku-Oki earthquake (M_w 9.0). In this case, the deformation that occurred in the ocean bottom is replaced by sea water, and the sea water change caused by the sea bottom displacement causes additional potential and gravity changes. However, the contribution of the sea water change to coseismic deformation cannot be modelled easily because of the irregular topography of the sea bottom. This sea water effect is essential and must be dealt with specially, so that the modelled coseismic deformation can be reasonably compared with GRACE data, because the seismic gravitational signal is dominated by the sea water correction that completely obscure the purely dislocation contribution. There are several methods to deal with the sea water correction.

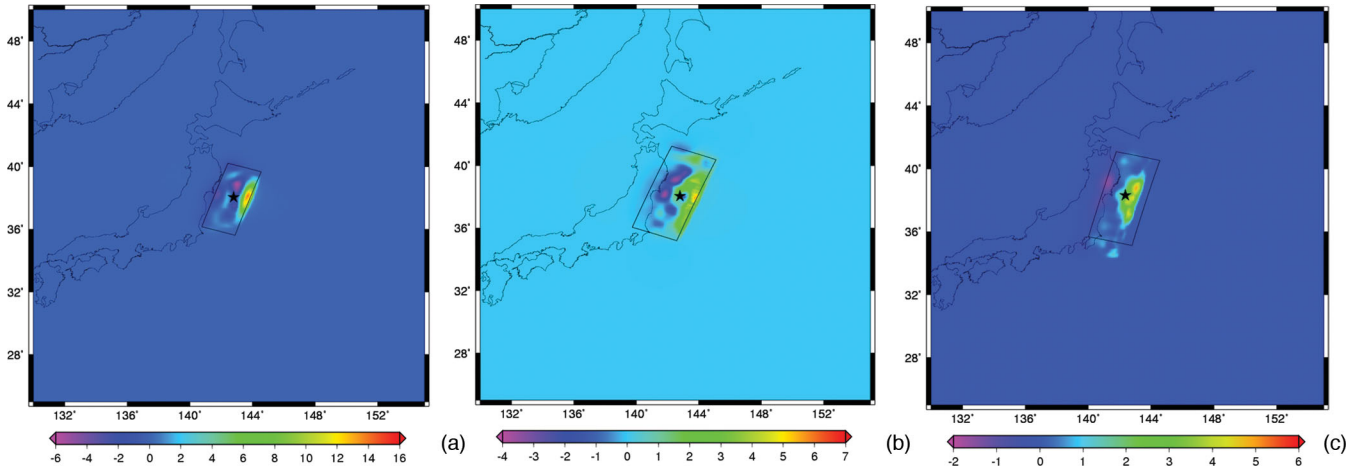

Figure 6. Vertical displacement caused by the 2011 Tohoku-Oki earthquake (M_w 9.0), calculated for three fault-slip models: (a) UCSB, (b) ARIA and (c) USGS. Unit: m.

The most simplified computing method was given by Heki & Matsuo (2010) who assumed a density contrast (between crustal rock and sea water) as the vertical deformation of the seafloor. This treatment is considered as a zero-order approximation. They considered the sea water contribution in their study of the coseismic gravity change caused by the 2010 Chile earthquake. Their results show that the sea water correction is important: the original gravity change profile had both positive and negative changes with comparable powers, but the negative change dominates after the correction.

A more reasonable and self-consistent approach was presented by Melini & Piersanti (2006) and Melini *et al.* (2010) with solving the complete seismic sea level equation. The sea surface deformation is described by the sea level equation that accounts for three effects: (i) the sea surface is an equipotential surface; (ii) the total sea water volume is conserved and (iii) the sea water redistribution causes a feedback load on the sea bottom that forces a further water redistribution and sea surface variations. Basically, an approximate approach is feasible, where (i) and (ii) must be considered although (iii) could be relaxed if the first-order approximation is made.

De Linage *et al.* (2009) considered the sea water correction from a different approach when they discussed the coseismic and post-seismic gravity change caused by the 2004 Sumatra earthquake (M_w 9.3). They computed the static potential perturbation of a global incompressible 3-km-thick ocean by imposing at its bottom the displacement field and potential perturbation. Cambiotti *et al.* (2011) also reported the coseismic gravity asymmetric pattern observed by GRACE is the result of the ocean water compensation other than the dilatation in the crust using ocean boundary conditions.

Recently, Broerse *et al.* (2011) treated the sea water contribution by means of solving the sea level equation on a spherical earth model gravitationally fully self-consistently, and applied it to the 2004 December 26 Sumatra–Andaman earthquake. They claimed a substantiation of the three important effects; they also show that to explain the GRACE observed gravity anomalies after the 2004 southeastern Asia earthquake, it is essential to gravitationally self-consistently solve the sea level equation, and the important role played by compressibility of the solid earth layers is detailed.

In this study, we apply an approximated approach to make sea water corrections. Sun *et al.* (2009) already solved the Poisson equation for the solid earth caused by a seismic source, and obtain the coseismic equipotential change on the earth surface, which is equivalent to the deformed sea level surface. Note that, although the solution of the Poisson equation is given for the solid earth, the earth's elastic deformation to a seismic source is dominating and essential, with respect to the sea water. On the other hand, once the solid earth has a coseismic deformation and produce a geopotential change (the equipotential change on surface is the sea level), the sea level naturally adjusts (by flowing) to be an equipotential surface. After the sea level adjustment, as the above studies (Melini & Piersanti 2006; Melini *et al.* 2010; Broerse *et al.* 2011) pointed out, the adjusted sea water produces a feedback load on the sea bottom that forces a further water redistribution and sea surface variations. However, the loading effect is a second-order perturbation, comparing to the sea water adjustment at the sea bottom. Therefore, in this study, we consider the direct contribution of the sea water change (adjustment) at the sea bottom to the coseismic geoid and vertical deflection changes, without an account for the second-order loading effect.

According to the numerical results presented by Broerse *et al.* (2011), the change in geoid height because of redistribution of water mass is about 30 times larger than the change in geoid height because of solid earth deformations caused by the changed water load on the crust (see fig. 5 in Broerse *et al.* 2011). This fact implies that the approximated result in our computation is at least one order larger than the second-order loading effect in amplitude. However, for a more precise estimate of the sea water correction to gravity, geoid and deflection changes, the above approaches by Melini & Piersanti (2006), Melini *et al.* (2010), De Linage *et al.* (2009) and Broerse *et al.* (2011) should be adopted.

To elucidate the sea water effects on coseismic geoid and deflection changes, we first compute the vertical displacements caused by the earthquake using the spherical dislocation theory and the computing program of Sun *et al.* (2009), for the three slip models. The modelled vertical displacements are depicted in Fig. 6, which shows the coseismic vertical displacements for the three slip models. The maximum displacement occurred in the ocean area, as is apparent for both positive and negative ones. However, the maximum displacements differ for the three models, as expected. The displacement for the USCB model ranges from –6 to +16 m. The displacement for the ARIA model is much smaller, ranging from –4 to 7 m. The displacement for Hayes (2011) shows similar deformation to that of the ARIA model displacement, ranging from –2 to 6 m.

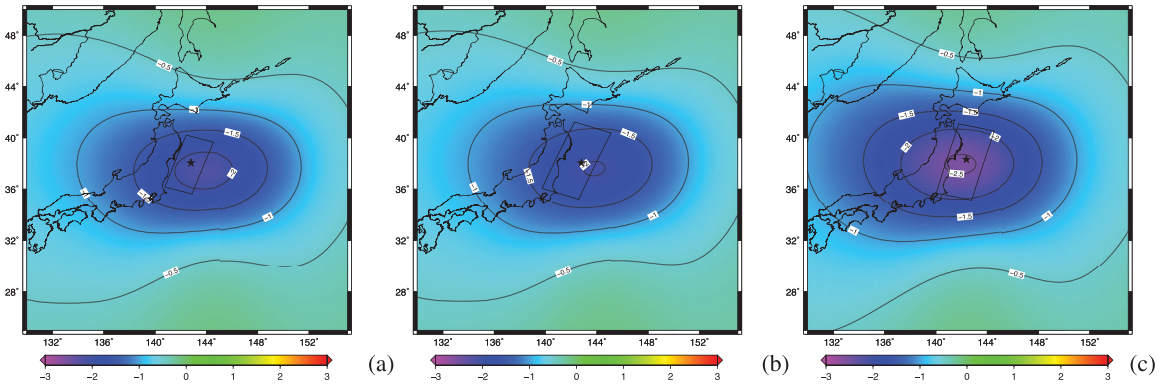

Figure 7. Sea water corrections to coseismic geoid changes with 350 km Gaussian filter for the UCSB (a), ARIA (b) and USGS (c) models. Unit: mm.

In computation of the sea water effects to the coseismic deformation, we must comprehensively consider the entire mass change of the sea water increase or decrease caused by the sea bottom vertical displacement instead of the density contrast between the crustal rock and sea water (Heki & Matsuo 2010) because the solid part of the earth model is already considered in the conventional dislocation theory. To compute the sea water contribution to coseismic gravity change, we might consider the vertical displacement beneath the computing point as a Bouguer layer according to the potential theory, so that the sea water correction can be estimated simply as

$$\delta g^{w.c.}(a,\theta,\varphi) = -2\pi G\rho_w u_r(a,\theta,\varphi), \tag{54}$$

where the superscript '$w.c.$' stands for sea water correction, G denotes the Newton's gravitational constant, $\rho_w = 1.03\mathrm{gcm}^{-3}$ represents the sea water density and $u_r(a,\theta,\varphi)$ is the coseismic vertical displacement as depicted in Fig. 6.

However, to make sea water correction to potential or geoid changes, the treatment presented above cannot be applied: the sea water change corresponding to the vertical displacement cannot be treated as a Bouguer layer (see chapter 3 in Heiskanen & Moritz 1967). In this case, we consider the spatial distribution of the sea water change, and compute the sea water correction to geoid and vertical deflection change by performing numerical integration as

$$\delta N^{w.c.}(a,\theta,\varphi) = -\frac{G}{g}\int_S \frac{\rho_w u_r(a,\theta',\varphi')}{l(\theta,\varphi;\theta',\varphi')}ds, \tag{55}$$

where $l(\theta,\varphi;\theta',\varphi')$ is the distance between the computing point and the displacement point, S is theoretically the whole ocean surface, but in practice it can be limited in the computing area. Similarly, the sea water corrections to the coseismic deflection change of the vertical are calculable as shown below:

$$\delta\xi^{w.c.}(a,\theta,\varphi) = \frac{1}{a}\frac{\partial\delta N^{w.c.}(a,\theta,\varphi)}{\partial\theta}, \tag{56}$$

$$\delta\eta^{w.c.}(a,\theta,\varphi) = -\frac{1}{a\sin\theta}\frac{\partial\delta N^{w.c.}(a,\theta,\varphi)}{\partial\varphi}. \tag{57}$$

Note that, in a practical computation using eqs (55)–(57), we compute the direct sea water correction of a layer of water of which the thickness is equal to the coseismic sea bottom displacement, assuming the water layer lies at the bottom of the ocean.

We consider a computing area bounded by longitude of 130°–155° and latitude of 25°–50°. We make numerical integration to compute the water corrections to coseismic geoid change using eq. (55) and to deflection change using eqs (56) and (57), with the vertical displacement data depicted in Fig. 6. The integration is limited only in the ocean area. The computed sea water corrections to the geoid change are depicted in Fig. 7; the sea water corrections to the deflection change are depicted in Fig. 8. The results are filtered using a Gaussian filter with an averaging radius of 350 km.

We learn from Fig. 7 that the sea water corrections to geoid change appear negative changes in the computing area. Then, they are almost identical magnitude and distribution pattern for the three slip models. However, the results indicate that the sea water correction (or effect) is very large; the maximum geoid change is about –2.0 to –2.5 mm near the epicentre.

Fig. 8 shows a very large sea water effect to the deflection change, reaching –1.0 to +0.7 mas for the $\delta\xi^{w.c.}$ component, and –0.8 to +0.8 mas for the $\delta\eta^{w.c.}$ component. The general distribution pattern appears to be similar among the three models, but the magnitude shows a large difference: the magnitude for the USGS model is remarkably larger than that for the other models; the negative correction (effect) is especially dominant over positive changes, which implies that the deflection change is sensitive to the earth models.

6 COSEISMIC DEFLECTION CHANGES CAUSED BY THE 2011 TOHOKU-OKI EARTHQUAKE (M_W 9.0)

6.1 GRACE-observed coseismic geoid and deflection changes

According to the computing scheme presented above, we first process the GRACE-observed data to obtain coseismic geoid and deflection vertical changes caused by the 2011 Tohoku-Oki earthquake (M_W 9.0). We use the GRACE Level 2 data sets composed of 60° Stokes' coefficients, released by Center for Space Research at the University of Texas. The length of data sets covers 103 months from 2002 October to 2011 May. We replaced the Earth's oblateness values (C_{20}) with those from satellite laser ranging (Cheng & Tapley 2004) because of their poor accuracy. Because geophysical effects such as ocean tide, solid Earth and ocean pole tides and atmosphere effect, have already been removed by modelling, the GRACE data sets are presumed to contain the coseismic deformation reflecting the mass redistribution. To reduce the significant longitudinal 'stripes', we apply a filtering scheme with decorrelation filtering P3M6 (remove a polynomial of 3° fitting for order 6 and above of Stokes' coefficients; Swenson & Wahr 2006) and 350 km Gaussian

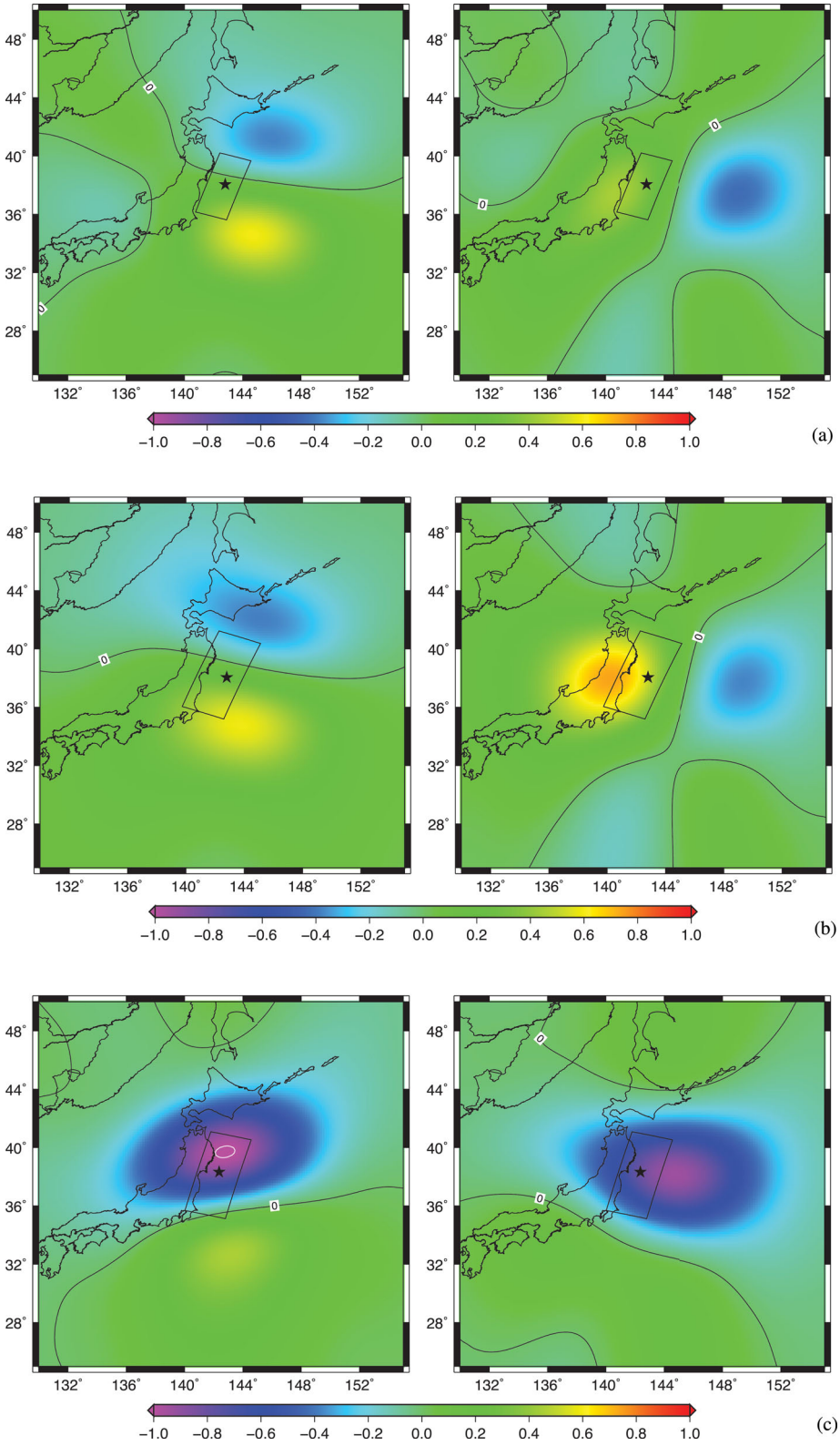

Figure 8. Sea water corrections to the deflection change of the vertical with 350 km Gaussian filter for UCSB (a), ARIA (b) and USGS (c) models. Unit: mas. The left subplot of each figure stands for the N–S component of deflection change $\delta\xi^{w.c.}$; the right one is the E–W component $\delta\eta^{w.c.}$.

smoothing. Such a filter radius with 350 km is reasonable because of the relation of Stokes coefficients degree and spatial resolution.

To extract the coseismic jumps from GRACE data, we first remove the seasonal and long-trend signals using least squares. Coseismic geoid and deflection change distribution is calculated and depicted in Fig. 9 respectively in the area of 130°–155° longitude and from 25°–50° latitude with a 0.5° × 0.5° grid, using the same filtering scheme and least-squares fitting. Fig. 9(a) shows dominat-

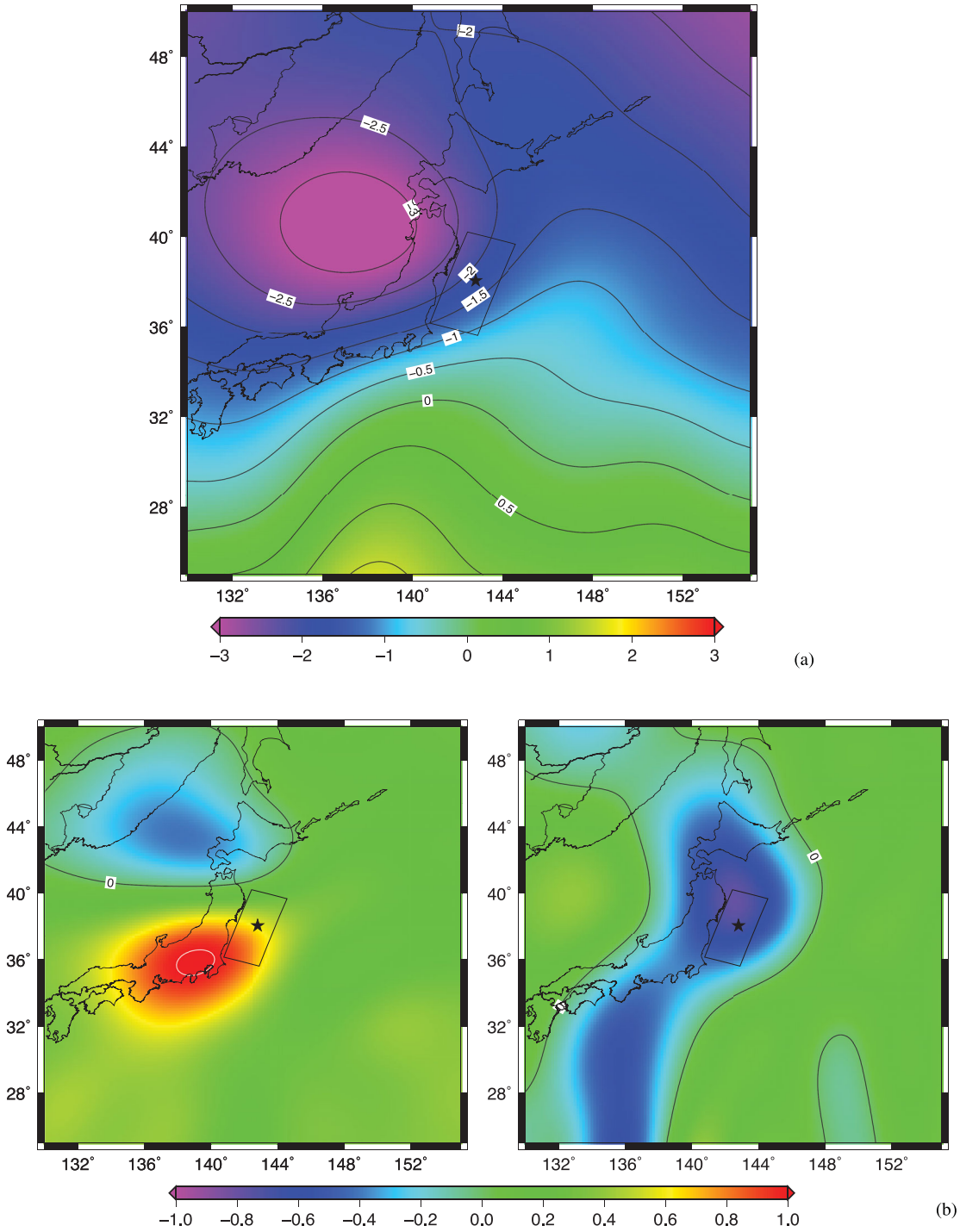

Figure 9. Coseismic geoid (a) and vertical deflection changes (b) measured by GRACE. The P3M6 and 350 km Gaussian filter are applied. Unit: mm for geoid and mas for deflection change. Black stars stand for the epicentre. In (b), the left subplot stands for the N–S component; whereas the right one is the E–W component.

ing negative geoid changes with approximately –3 mm maximum change in the Sea of Japan area; although the positive changes in the southern area to Japan are small. The N–S component of deflection change (Fig. 9b left subplot) shows equivalent magnitudes of positive and negative changes; whereas the E–W component (Fig. 9b right subplot) shows dominating negative changes.

6.2 Modelled coseismic geoid and deflection changes on solid surface

Then we compute the theoretical coseismic geoid and deflection changes using the computing scheme described as a result of this study, with the three slip models presented above in Fig. 5. To compare the modelled coseismic deformation with the GRACE-observed ones (Fig. 9), the dislocation Love numbers are truncated

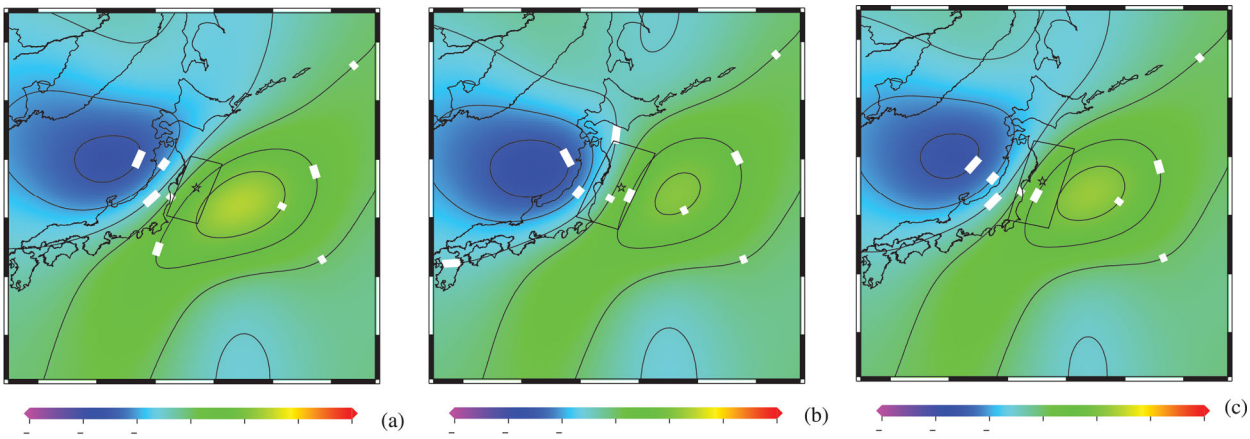

Figure 10. Modelled geoid change caused by the 2011 Tohoku-Oki earthquake for UCSB (a), ARIA (b) and USGS (c) models; results are smoothed by the 350 km Gaussian filter. Unit: mm.

at 60° in computing Green's functions, and the P3M6 and 350 km smoothing Gaussian filter are applied. The modelled geoid changes are depicted in Fig. 10; the deflection changes are depicted in Fig. 11. The modelled geoid changes for the three fault-slip models are identical, ranging from –2.0 to +1.5 mm, almost identical in magnitude and distribution pattern, which implies that the geoid changes are not sensitive to the fault-slip models. However, comparison of the modelled geoid change (Fig. 10) and the GRACE-observed one (Fig. 9a) reveals a big difference between them. Actually, as shown below, this difference is mainly caused by the sea water effects.

Similarly, the distribution of the deflection changes in Fig. 11 for the three slip models are fundamentally the same in magnitude and distribution pattern. However, they appear to be more different than the geoid changes in spatial distribution, and more different among the three slip models. This phenomenon can be considered as attributable to the following fact: the deflection is a mathematical differential of geoid (ref. eqs (6) and (7)), so that it is naturally sensitive to the high-frequency part.

6.3 Coseismic geoid and deflection changes after sea water correction

As discussed above, the modelled coseismic deformation must be corrected for the sea water change caused by the sea bottom displacement. Therefore, we correct the computed coseismic geoid changes by adding the sea water corrections, and we then obtain the final coseismic geoid changes caused by the 2011 Tohoku-Oki earthquake (M_w 9.0) for the three slip models. The results depicted in Fig. 12 show that the final coseismic geoid changes are dominated by negative changes, reaching about –3.0 mm, and coincides with the GRACE-observed one (Fig. 9a). Considering the sea water correction changes, the distribution pattern of the coseismic geoid change from equivalent negative and positive geoid change to negative dominating geoid change, it might be concluded that the sea water effect is too large to ignore to model the coseismic deformations correctly. To explicitly show how the modelled geoids agree with the GRACE-observed one, the corresponding differences are plotted in Figs 12(d)–(f). It is seen that the difference is pretty small. The slight difference around the edge of the study area is regarded as resulting from truncation error in theoretical computation and the oceanic disturbance in GRACE data. Again, the magnitude and spatial distribution pattern for the three slip models are almost identical because they mutually agree, which implies that the coseismic geoid change is not sensitive to the fault-slip model.

We obtain the final coseismic deflection changes by adding the sea water corrections to the modelled ones. The results are shown, respectively, in Fig. 13 for the three fault-slip models. The figure shows that the magnitude and distribution pattern of the N–S component of the deflection changes for the first two models are almost identical to the GRACE-observed one, but the N–S component for the USGS model and the entire E–W component shows large differences in the distribution pattern with the GRACE-observed deflection change. This difference might result from two reasons. One reason is that the GRACE orbit, which flies nearly the N–S direction, the observation accuracy along the N–S direction is naturally higher than that of E–W direction, that is, the E–W component of the observed deflection change in Fig. 9(b) contains larger error than the N–S component (Fig. 9a). Another reason might be the error of the fault-slip model. Carefully comparing the E–W components of the three slip models in Fig. 13 reveals that their distribution patterns differ completely: positive deflection change is dominant for the UCSB and ARIA models (Figs 13a and b), but negative deflection change is dominant for the USGS model (Fig. 13c). This phenomenon shows that the deflection change is sensitive to the fault-slip model, which might be beneficial when we use GRACE data to invert the fault-slip model because it can provide a sensitive constraint. The conclusion is confirmed by their explicit differences with the GRACE-observed ones as shown in Fig. 14.

The comparison of the three fault-slip models leads to the result that the USGS model is less good with respect to the GRACE data. It might be considered because of the different seismic data source used for the three models. The first two fault-slip models were obtained based on the Japan Meteorological Agency (JMA) hypocentre (Lon. = 142.8° Lat. = 38.05° depth = 24 km), although the USGS model was obtained based on the USGS hypocentre (Lon. = 142.37° Lat. = 38.32° depth = 30 km). It is seen that the two hypocentres are different by 0.43° in longitude and 0.27° in latitude; in addition, the depth of the source is also different by 6 km. The other possible reasons of the difference remains to be further investigated and discussed in the future.

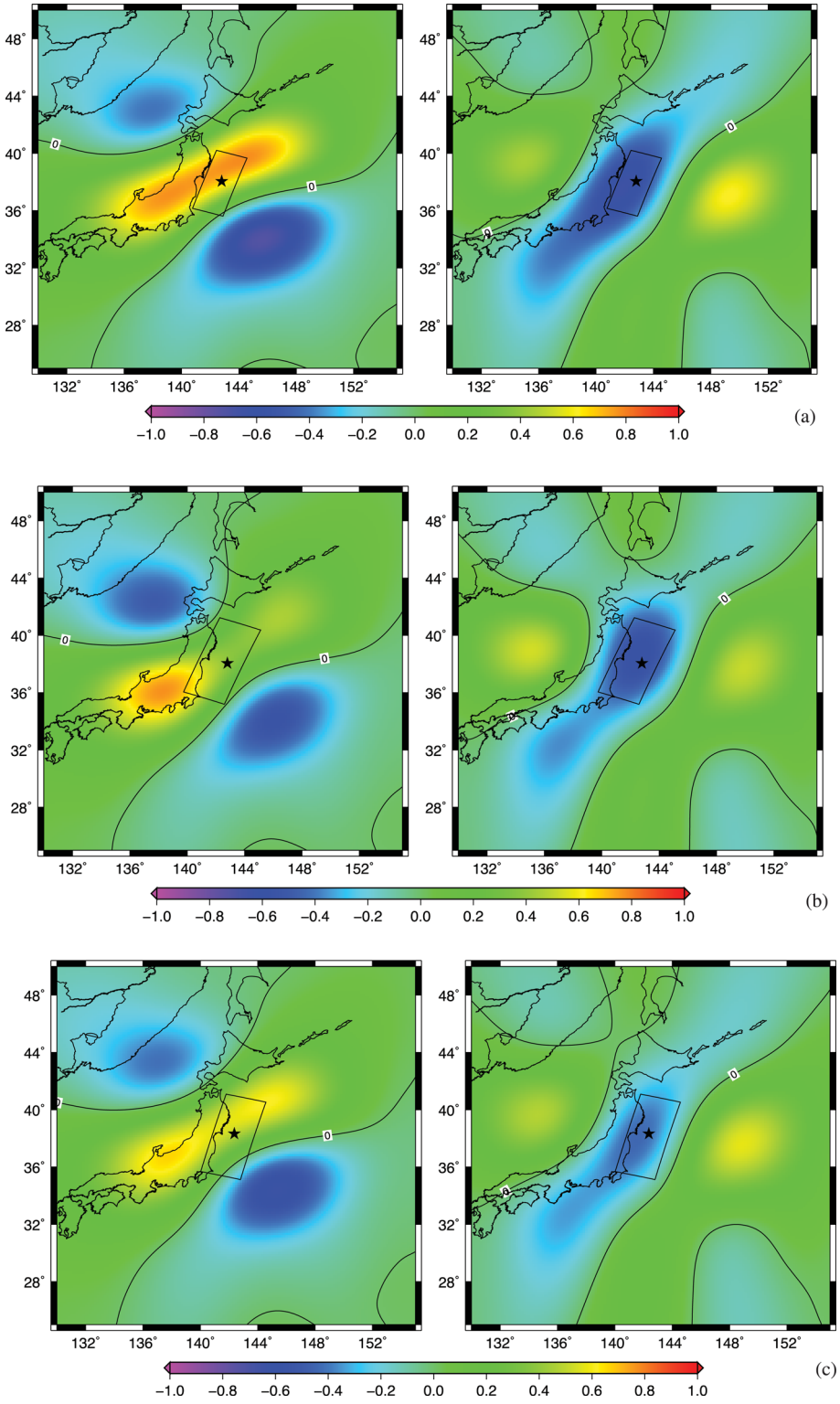

Figure 11. Modelled deflection change of the vertical caused by the 2011 Tohoku-Oki earthquake for UCSB (a), ARIA (b) and USGS (c) models; results are smoothed by the 350 km Gaussian filter. The left subplot of each figure stands for the N–S component of deflection change; the right one is the E–W component. Unit: mas.

6.4 Deflection change vector caused by the earthquake

Finally, we convert the two components of the deflection changes into a vector form for the GRACE-observed and modelled ones depicted in Fig. 15. The GRACE-observed deflection change (Fig. 15a) shows that the maximum change occurs in the Japanese mainland, moving fundamentally northward; the results for UCSB and ARIA models are almost identical, mainly occurring in the Japanese mainland. However, the direction of motion appears somewhat different from the GRACE-observed one. The

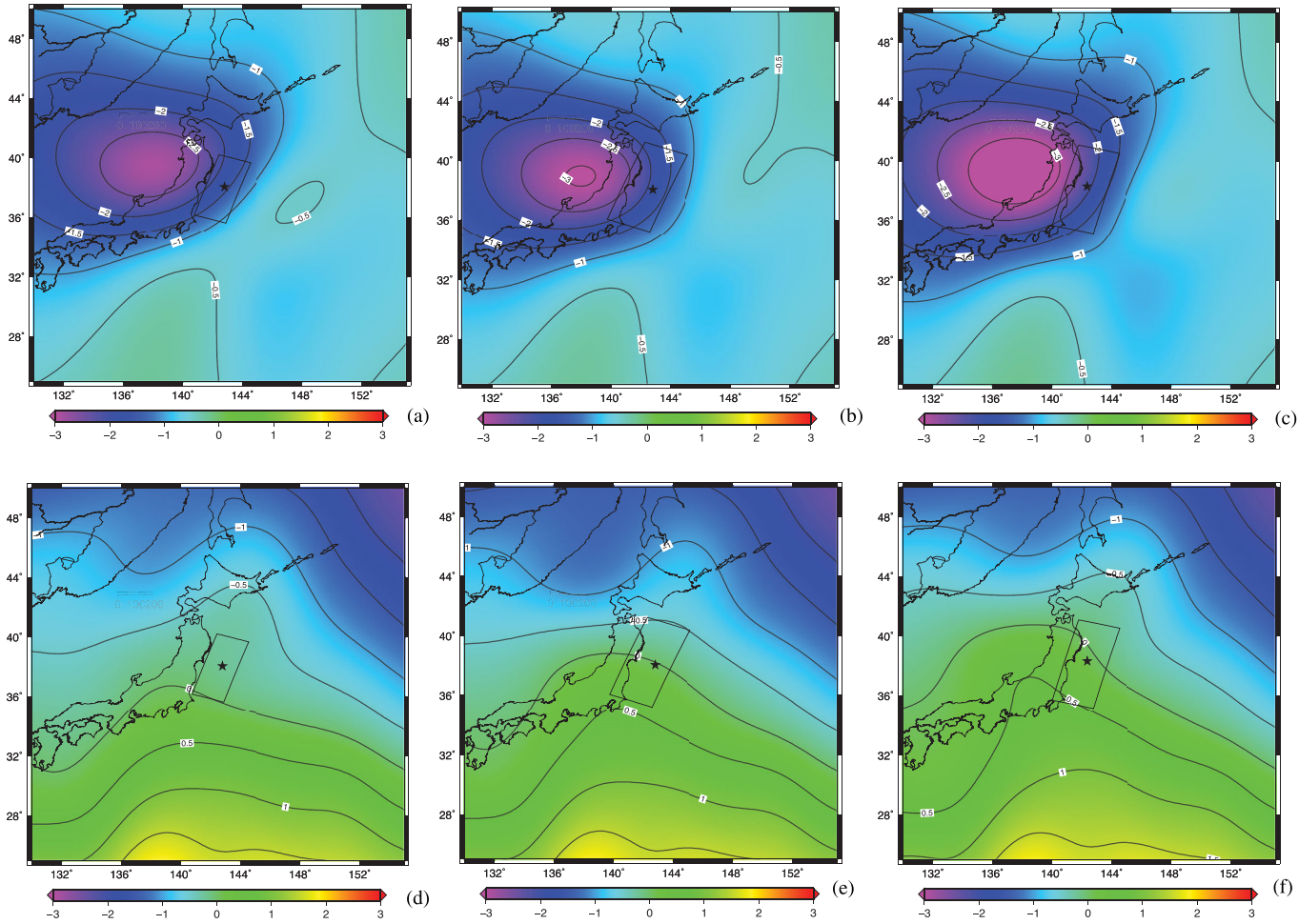

Figure 12. Final coseismic geoid changes after sea water correction for the three slip models of UCSB (a), ARIA (b) and USGS (c): all are smoothed by a Gaussian filter with an averaging radius of 350 km; Panels (d)–(f) show respectively the corresponding differences between the three modelled geoid changes and the GRACE observed ones. Unit: mm.

deflection change for the USGS model indicates a big difference from the other two models and the GRACE-observed one.

7 CONCLUDING REMARKS

In this paper, we presented a scheme to compute coseismic deflection change of the vertical, and derive a set of Green's functions for four independent dislocation sources. These Green's functions are used to compute deflection changes caused by an arbitrary seismic source located anywhere on the earth, through a proper combination of the four independent solutions. To compare the theoretical deflection change with the GRACE-observed ones, we truncate the dislocation Love numbers and compute the Green's functions with Gaussian filter applied, so that we might save much unnecessary computing time for the high-degree Love numbers. Numerical comparison demonstrates that the computing scheme is both valid and efficient.

We considered the problem of sea water correction to modelled geoid and deflection changes. This sea water correction is an important and necessary step to compare the modelled results with GRACE-observed deformations. The conventional dislocation theory is usually valid for a solid elastic earth, so that the surface uplift on earth surface is replaced with air. However, for a large earthquake occurring in or near an oceanic area, the deformation that occurred in the ocean bottom is replaced by sea water, and the sea bottom displacement causes additional potential and gravity changes. This sea water effect must be addressed specially, so that the modelled coseismic deformation can be compared reasonably with GRACE data. We discussed how to make sea water corrections to the potential/geoid and deflection changes because the treatment differs from that of gravity. Furthermore, we conclude that the ocean contribution can change the modelled coseismic gravity pattern on the solid earth surface and is a major signal observed by GRACE for the Tohoku-Oki earthquake. It should be pointed out that because GRACE gives each single harmonic component of the potential, it is possible to compare separately the contribution from each harmonic component before summing. However, because of the volume limit of the paper, the detailed discussion of this topic remains for further investigation in the future.

As an application of the dislocation theory and the computing scheme described as a result of this study, we consider the 2011 Tohoku-Oki earthquake (M_w 9.0) using three different fault-slip models. Using the fault models, we compute the coseismic geoid and deflection changes for an area around Japan. We then compute the sea water corrections for geoid and deflection changes. After the sea water correction, the modelled coseismic geoid and

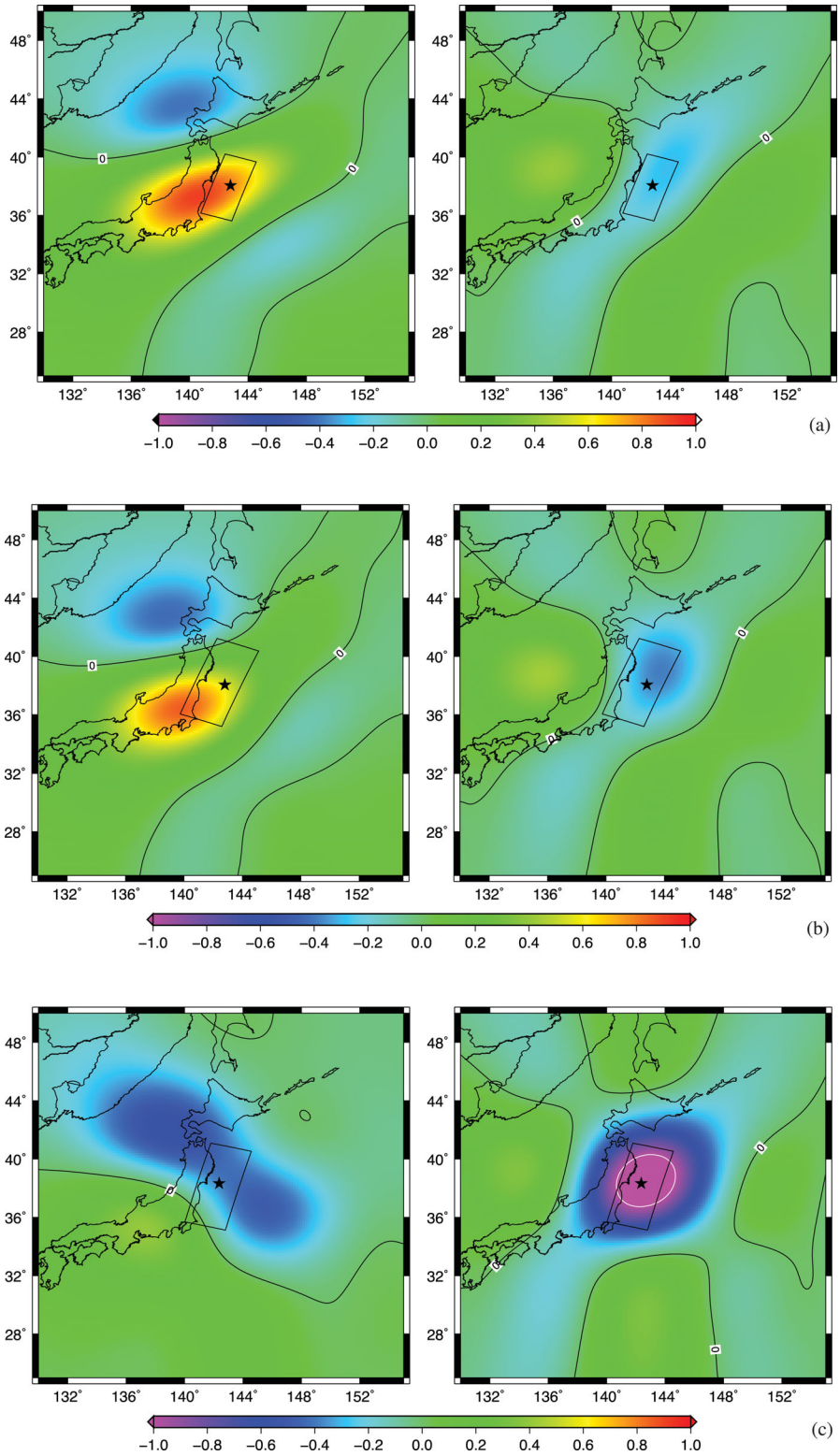

Figure 13. Final coseismic vertical deflection changes after sea water corrections caused by the 2011 Tohoku-Oki earthquake (M_w 9.0) for the three fault-slip models of UCSB (a), ARIA (b) and USGS (c). They are smoothed by the Gaussian filter with average radius of 350 km. The left subplot of each figure stands for the N–S component of the deflection change; whereas the right subplot is the E–W component. Unit: mas.

deflection changes indicate that both the coseismic geoid and deflection changes can be detected clearly by GRACE observation. Results show that the coseismic geoid change is not sensitive to the fault-slip models: the three slip models yield identical coseismic geoid changes, although the coseismic deflection changes are very sensitive to the fault-slip models because the modelled deflection changes indicate a large difference, especially for the E–W component. These behaviours provide a new and useful approach to invert

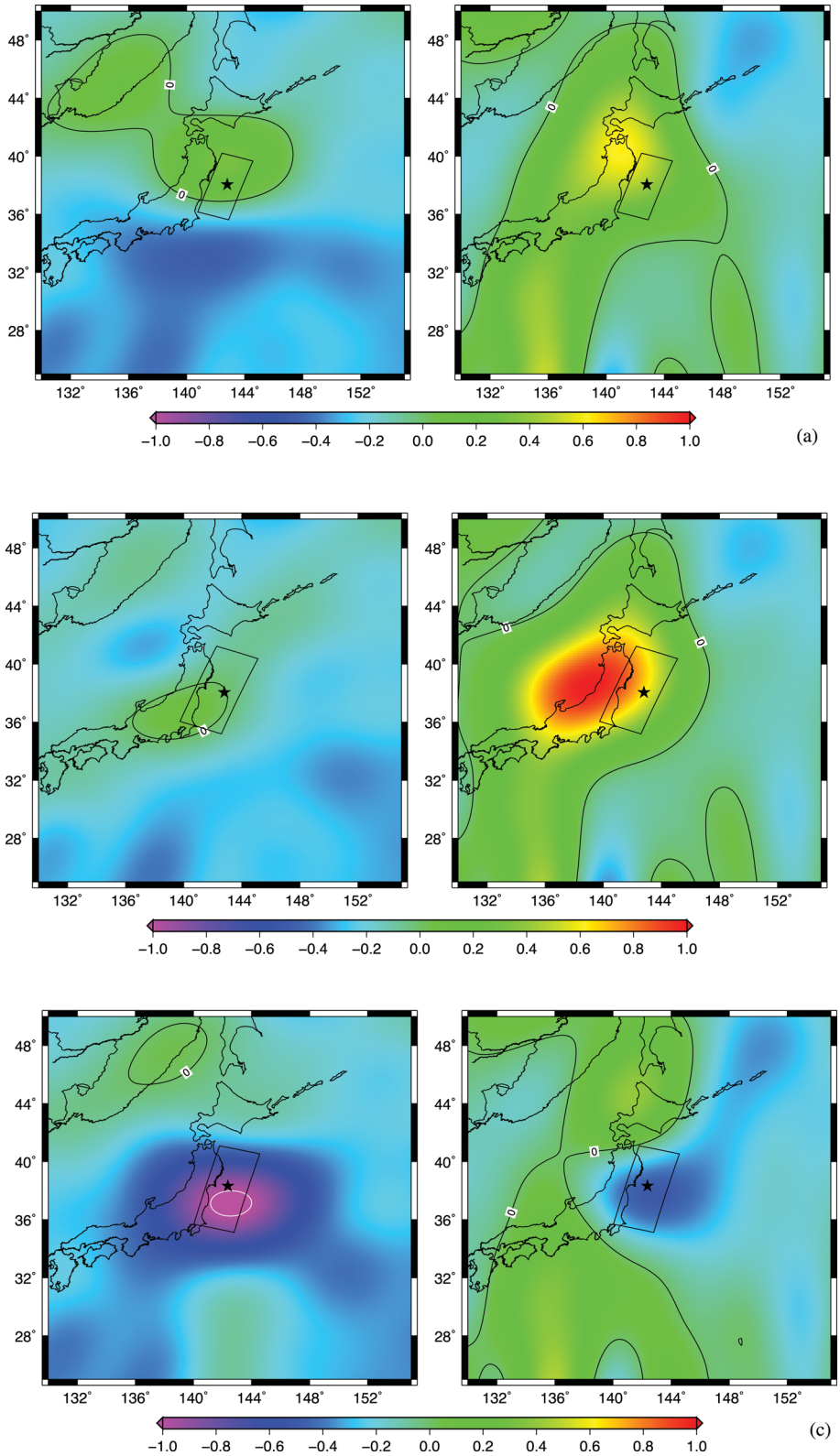

Figure 14. Differences between the coseismic vertical deflection changes after sea water corrections and the GRACE-observed ones caused by the 2011 Tohoku-Oki earthquake (M_w 9.0) for the three fault-slip models of UCSB (a), ARIA (b) and USGS (c), respectively. They are smoothed by the Gaussian filter with average radius of 350 km. The left subplot of each figure stands for the N–S component of the deflection change; whereas the right subplot is the E–W component. Unit: mas.

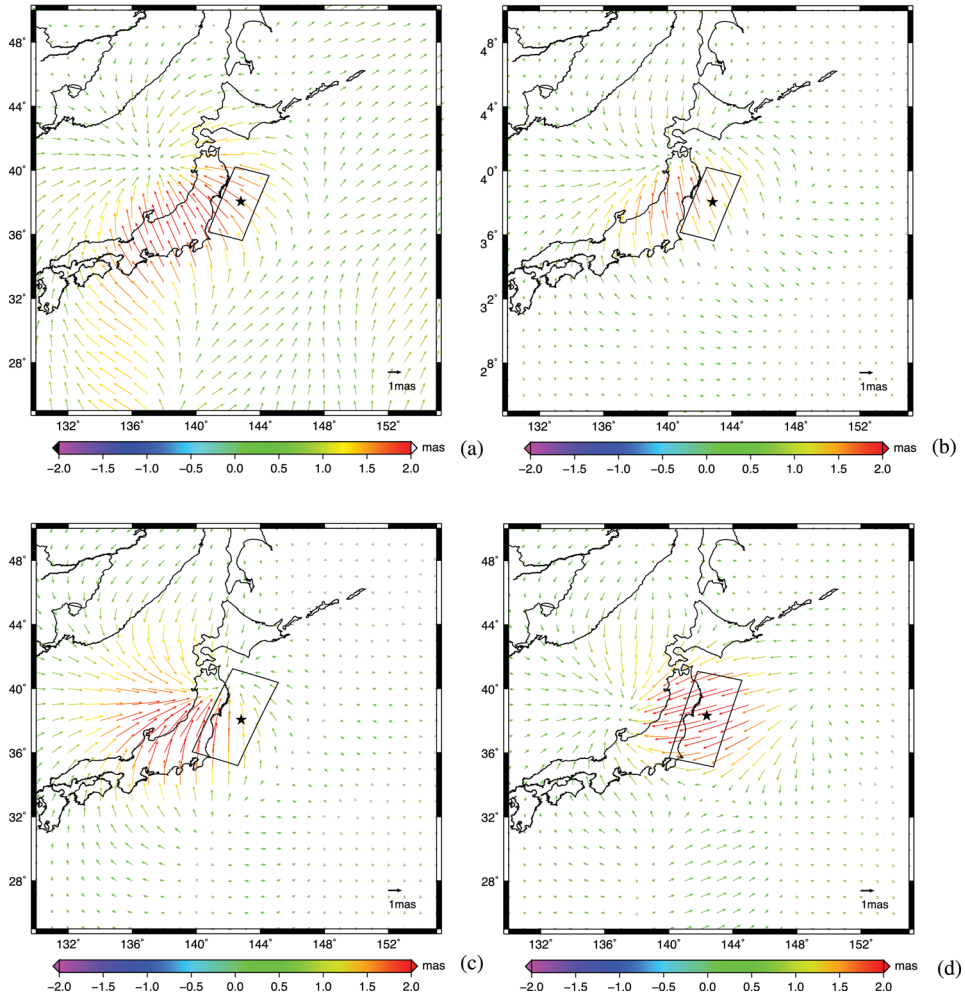

Figure 15. Vector form of the deflection vertical changes caused by the 2011 Tohoku-Oki earthquake (M_w 9.0) for GRACE data (a), UCSB model (b), ARIA model (c) and the USGS model (d). Unit: mas.

the seismic fault using GRACE-observed deflection changes as a constraint.

ACKNOWLEDGMENTS

The authors are grateful to the Editor (Bert Vermeersen) and two anonymous reviewers for their helpful and constructive comments which greatly improved the paper. This study was financially supported by National Nature Science Foundation of China (Grant No. 41174063).

REFERENCES

Ammon, C.J. *et al*., 2005. Rupture process of the 2004 Sumatra–Andaman earthquake, *Science,* **308,** 1133–1139.

Banerjee, P., Pollitz, F.F. & Burgmann, R., 2005. The size and duration of the Sumatra–Andaman earthquake from far-field static offsets, *Science,* **308,** 1769–1772.

Boschi, E., Casarotti, E., Devoti, R., Melini, D., Piersanti, A., Pietrantonio, G. & Riguzzi, F., 2006. Coseismic deformation induced by the Sumatra earthquake, *J. Geodyn.,* **42,** 52–62.

Broerse, D.B.T., Vermeersen, L.L.A., Riva, R.E.M. & van der Wal, W., 2011. Ocean contribution to co-seismic crustal deformation and geoid anomalies: application to the 2004 December 26 Sumatra–Andaman earthquake, *Earth planet. Sci. Lett.,* **305,** 341–349.

Cambiotti, G., Bordoni, A., Sabadini, R. & Colli, L., 2011. GRACE gravity data help constraining seismic models of the 2004 Sumatra earthquake, *J. geophys. Res.,* **116,** B10403, doi:10.1029/2010JB007848.

Cannelli, V., Melini, D., Piersanti, A. & Boschi, E., 2008. Postseismic signature of the 2004 Sumatra earthquake on low-degree gravity harmonics, *J. geophys. Res.,* **113,** B12414, doi:10.1029/2007JB005296.

Chen, J.L., Wilson, C.R., Tapley, B.D. & Grand, S., 2007. GRACE detects coseismic and postseismic deformation from the Sumatra–Andaman earthquake, *Geophys. Res. Lett.,* **34,** L13302, doi:10.1029/2007GL030356.

Cheng, M. & Tapley, B.D., 2004. Variations in the Earth's oblateness during the past 28 years, *J. geophys. Res.,* **109,** B09402, doi:10.1029/2004JB003028.

Dahlen, F. A., 1968. The normal modes of a rotating, elliptical Earth. *Geophys. J. R. astron. Soc.,* **16,** 329–367, doi: 10.1111/j.1365-246X.1968.tb00229.x.

De Linage, C., Rivera, L., Hinderer, J., Boy, J.-P., Rogister, Y., Lambotte S. & Biancale R., 2009. Separation of coseismic and postseismic gravity changes for the 2004 Sumatra–Andaman earthquake from 4.6 yr of GRACE observations and modelling of the coseismic change by normal–modes summation, *Geophys. J. Int.,* **176**(3), 695–714.

Dziewonski, A.M. & Anderson, D.L., 1981. Preliminary reference earth model, *Phys. Earth planet. Inter.,* **25,** 297–356.

Fu, G. & Sun, W., 2006. Global co-seismic displacements caused by the 2004 Sumatra–Andaman earthquake (M_w 9.1), *Earth Planets Space,* **58,** 149–152.

Gross, R.S. & Chao, B.F., 2001. The gravitational signature of earthquakes, in *Gravity, Geoid, and Geodynamics 2000,* pp. 205–210, IAG Symposia Vol. 123, ed. Sideris, M.G., Springer-Verlag, New York, NY.

Han, S.-C., Shum, C.K., Bevis, M., Ji, C. & Kuo, C.-Y., 2006. Crustal dilatation observed by GRACE after the 2004 Sumatra-Andaman earthquake, *Science,* **313,** 658–662.

Han, S.-C., Sauber, J. & Luthcke, S., 2010. Regional gravity decrease after the 2010 Maule (Chile) earthquake indicates large-scale mass redistribution, *Geophys. Res. Lett.,* **37,** L23307, doi:10.1029/2010GL045449.

Hayes, G., 2011. Finite fault model updated result of the March 11, 2011 M_w 9.0 earthquake offshore Honshu, Japan. Available at http://earthquake.usgs.gov/earthquakes/eqinthenews/2011/usc0001xgp/finite_fault.php.

Heiskanen, W.A. & Moritz, H., 1967. *Physical Geodesy,* Freemen, San Francisco.

Heki, K. & Matsuo, K., 2010. Coseismic gravity changes of the 2010 earthquake in Central Chile from 163 satellite gravimetry, *Geophys. Res. Lett.,* **37,** L24306, doi:10.1029/2010GL045335.

Imanishi, Y., Sato, T., Higashi, T., Sun, W. & Okubo, S., 2004. A Network of superconducting gravimeters detects submicrogal coseismic gravity changes, *Science,* **306,** 476–478.

Irwan, M., Kimata, F., Hirahara, K., Sagiya, T. & Yamagiwa, A., 2004. Measuring ground deformations with 1-second sampled GPS data: the 2003 Tokachi-oki earthquake (preliminary report), *Earth Planets Space,* **56,** 389–393.

Jekeli, C., 1981. Alternative methods to smooth the Earth's gravity field Report 327, Department of Geodynamic Science and Survey, Ohio State University, Columbus.

Khan, S.A. & Gudmundsson, O., 2005. GPS analyses of the Sumatra–Andaman earthquake, *EOS, Trans. Am. geophys. Un.,* **86**(9), 89, doi:10.1029/2005EO090001.

Lin, A., Fu, B., Guo, J., Zeng, Q., Dang, G., He, W. & Zhao, Y., 2002. Co-seismic strike-slip and rupture length produced by the 2001 Ms 8.1 Central Kunlun Earthquake, *Science,* **296,** 1917–2088.

Ma, X.Q. & Kusznir, N.J., 1994. Effects of rigidity layering, gravity and stress relaxation on 3-D subsurface fault displacement fields, *Geophys. J. Int.,* **118,** 201–220.

Matsuo, K. & Heki, K., 2011. Coseismic gravity changes of the 2011 Tohoku-Oki earthquake from satellite gravimetry, *Geophys. Res. Lett.,* **38,** L00G12, doi:10.1029/2011GL049018.

Melini, D. & Piersanti, A., 2006. Impact of global seismicity on sea level change assessment, *J. geophys. Res.,* **111**(B03406), 14, doi:10.1029/2004JB003476.

Melini, D., Spada, G. & Piersanti, A., 2010. A sea level equation for seismic perturbations, *Geophys. J. Int.,* **180,** 88–100, doi:10.1111/j.1365-246X.2009.04412.x.

Mikhailov, V., Tikhotsky, S., Diament, M., Panet, I. & Ballu, V., 2004. Can tectonic processes be recovered from new gravity satellite data? *Earth planet. Sci. Lett.,* **228,** 281–297, doi:10.1016/j.epsl.2004.09.035.

Ogawa, R. & Heki, K., 2007. Slow postseismic recovery of geoid depression formed by the 2004 Sumatra–Andaman earthquake by mantle water diffusion, *Geophys. Res. Lett.,* **34,** L06313, doi:10.1029/2007GL029340.

Okada, Y., 1985. Surface deformation caused by shear and tensile faults in a half-space, *Bull. seism. Soc. Am.,* **75**(4), 1135–1154.

Okubo, S., 1991. Potential and gravity changes raised by point dislocations, *Geophys. J. Int.,* **105,** 573–586.

Okubo, S., 1992. Potential and gravity changes caused by shear and tensile faults, *J. geophys. Res.,* **97,** 7137–7144.

Okubo, S., 1993. Reciprocity theorem to compute the static deformation due to a point dislocation buried in a spherically symmetric Earth, *Geophys. J. Int.,* **115,** 921–928.

Panet, I. *et al*., 2007. Coseismic and post-seismic signatures of the Sumatra 2004 December and 2005 March earthquakes in GRACE satellite gravity, *Geophys. J. Int.,* **171**(1), 177–190.

Piersanti, A., Spada, G., Sabadini, R. & Bonafede, M., 1995. Global postseismic deformation, *Geophys. J. Int.,* **120,** 544–566.

Pollitz, F.F., 1992. Postseismic relaxation theory on the spherical Earth, *Bull. seism. Soc. Am.,* **82,** 422–453.

Rundle, J.B., 1982. Viscoelastic gravitational deformation by a rectangular thrust fault in a layered Earth, *J. geophys. Res.,* **87,** 7787–7796.

Sabadini, R., Piersanti, A. & Spada, G., 1995. Toroidal/poloidal partitioning of global post-seismic deformation, *Geophys. Res. Lett.,* **21,** 985–988.

Saito, M., 1967. Excitation of free oscillations and surface waves by a point source in a vertically heterogeneous Earth, *J. geophys. Res.,* **72,** 3689–3699.

Saito, M., 1974. Some problems of static deformation of the earth, *J. Phys. Earth,* **22,** 123–140.

Shao, G., Li, X., Ji, C. & Maeda, T., 2011. Preliminary result of the March 11, 2011 M_w 9.1 Honshu Earthquake. Available at http://www.geol.ucsb.edu/faculty/ji/big_earthquakes/2011/03/0311_v3/Honshu.html (last accessed 2012 January 20).

Smylie, D.S. & Mansinha, L., 1971. The elasticity theory of dislocation in real Earth models and changes in the rotation of the Earth, *Geophys. J. R. astr. Soc.,* **23,** 329–354.

Soldati, G., Piersanti, A. & Boschi, E., 1998. Global postseismic gravity changes of a viscoelastic Earth, *J. geophys. Res.,* **103**(B12), 29 867–29 886, doi:10.1029/98JB02793.

Sun, W., 1992a. Potential and gravity changes raised by dislocations in spherically symmetric Earth models, *PhD thesis*, University of Tokyo, Japan.

Sun, W., 1992b. Potential and gravity changes caused by dislocations in spherically symmetric Earth models, *Bull. Earthq. Res. Inst. Univ. Tokyo,* **67,** 89–238.

Sun, W. & Okubo, S., 1993. Surface potential and gravity changes due to internal dislocations in a spherical Earth—I. Theory for a point dislocation, *Geophys. J. Int.,* **114,** 569–592.

Sun, W. & Okubo, S., 2004. Co-seismic deformations detectable by satellite gravity missions—a case study of Alaska (1964, 2002) and Hokkaido (2003) earthquakes in the spectral domain, *J. geophys. Res.,* **109,** B4, B04405, doi:10.1029/2003JB002554.

Sun, W., Okubo, S. & Vanicek, P., 1996. Global displacement caused by dislocations in a realistic earth model, *J. geophys. Res.,* **101,** 8561–8577.

Sun, W., Okubo, S. & Fu, G., 2006. Green's function of co-seismic strain changes and investigation of effects of Earth's curvature and radial heterogeneity, *Geophys. J. Int.,* **167,** 1273–1291, doi:10.1111/j.1365-246X.2006.03089.x.

Sun, W., Okubo, S., Fu, G. & Araya, A., 2009. General formulations of global co-seismic deformations caused by an arbitrary dislocation in a spherically symmetric earth model—applicable to deformed earth surface and space-fixed point, *Geophys. J. Int.,* **177,** 817–833, doi:10.1111/j.1365-246X.2009.04113.x.

Swenson, S.C. & Wahr, J., 2006. Post-processing removal of correlated errors in GRACE data, *Geophys. Res. Lett.,* **33,** L08402, doi:10.1029/2005GL025285.

Takeuchi, H. & Saito, M., 1972. Seismic surface waves, *Methods Comput. Phys.,* **11,** 217–295.

Tanaka, Y., Okuno, J. & Okubo, S., 2006. A new method for the computation of global viscoelastic post-seismic deformation in a realistic earth model (I)—vertical displacement and gravity variation, *Geophys. J. Int.,* **164**(2), 273–289.

Vigny, C. *et al*., 2005. Insight into the 2004 Sumatra–Andaman earthquake from GPS measurements in Southeast Asia, *Nature,* **436,** 201–206.

Wahr, J., Molenaar, M. & Bryan, F., 1998. Time variability of the Earth's gravity field: hydrological and oceanic effects and their possible detection using GRACE, *J. geophys. Res.,* **103,** 30 205–30 230.

Wang, R., Lorenzo-Martin, F. & Roth, F., 2006. PSGRN/PSCMP—a new code for calculating coseismic and post-seismic deformation, geoid and gravity changes based on the viscoelastic-gravitational dislocation theory, *Comput. Geosci.,* **32,** 527–541.

Wei, S., Sladen, A. & the ARIA group, 2011. Updated result 3/11/2011 (M_w 9.0), Tohoku-oki, Japan. Available at:

http://www.tectonics.caltech.edu/slip_history/2011_taiheiyo-oki/ (last accessed 2012 January 20).

Yang, M., Juin, R., Yu, J., Yu, J. Yih & Yu, T. To, 2000. Geodetically observed surface displacements of the 1999 Chi–Chi, Taiwan earthquake, *Earth Planets Space,* **52,** 403–413.

Yu, S.B. *et al*., 2001. Preseismic deformation and coseismic displacements associated with the 1999 Chi–Chi, Taiwan, earthquake, *Bull. seism. Soc. Am.,* **91,** 995–1012.

Zhou, X., Sun, W., Zhao, B., Fu, G., Dong, J. & Nie, Z., 2011a. Geodetic observations detected co-seismic displacements and gravity changes caused by the Tohoku-Oki earthquake ($M_w = 9.0$), *J. geophys. Res.,* submitted.

Zhou, X., Sun, W. & Fu, G., 2011b. Gravity satellite GRACE detects coseismic gravity changes caused by 2010 Mw 8.8 Chile earthquake, *Chin. J. Geophys.*, **54**(7), 1745–1749, doi:10.3969/j.issn.0001-5733.2011.07.007 (in Chinese).